

Construction of 3D printed reduced-fat meat analogue by emulsion gels. Part II: Printing performance, thermal, tribological, and dynamic sensory characterization of printed objects

Mahdiyaz Shahbazi^{a,*}, Henry Jäger^{a,**}, Jianshe Chen^b, Rammile Ettelaie^c

^a Institute of Food Technology, University of Natural Resources and Life Sciences (BOKU), Muthgasse 18, 1190, Vienna, Austria

^b Food Oral Processing Laboratory, School of Food Science & Biotechnology, Zhejiang Gongshang University, Hangzhou, China

^c Food Colloids and Bioprocessing Group, School of Food Science and Nutrition, University of Leeds, Leeds, LS2 9JT, UK

ARTICLE INFO

Keywords:

Meat analogue
3D printing
Biosurfactant
DSC
Oral tribology
Temporal dominance of sensations

ABSTRACT

The manufacture of a high-quality meat analogue needs the utilization of appropriate ingredients through the application of cutting-edge technology to mimic the functional properties of traditional meat without negatively affecting the product features. Here, the reduced-fat soy-based emulsion gels, prepared by biosurfactant variants, were printed via an extrusion-based printer to manufacture a well-defined 3D structure. The printing performance revealed the 3D printed meat analogues formulated by dodecyl succinylated inulin and ethyl (hydroxyethyl) cellulose presented a finer resolution compared to acetylated and octenyl succinic anhydride modified starches. The microstructure images provided evidence for the formation of an interconnected network with a highly porous structure in the 3D printed samples. Thermal and crystalline behaviors showed that the biosurfactants affected the crystalline structure, offering an increase in the hardness. The oral tribology measurements lead to the conclusion that the presence of biosurfactants reduced the friction coefficients. The presence of a large quantity of aggregated proteins was related to the possible formation of hydrogen bonds between the protein molecules. Moreover, disulfide bonds became progressively important in the samples, including modified inulin and modified cellulose, initiating the development of the fibrous structure. Temporal dominance of sensations also indicated that the biosurfactants induced a fibrous sensation in the printed meat analogues. The results of this study demonstrated how the application of emulsion gels in 3D printing process can further produce reduced-fat meat analogues with desired 3D structure and modified textures for enhanced eating experiences.

1. Introduction

The 3D printing, otherwise called rapid prototyping, consists of fabricating solid 3D architectures from virtual models with a computer-aided design (CAD) software, where the CAD model is converted into STL (Standard Triangular Language) file format to design digital models (Van der Linden, 2015). The implementation of the 3D printing technique in food manufacturing has developed the most important innovations in the food industry towards the development of personalized and custom-designed foods, including creating products with intricate shapes and complex geometries, facilitating supply chain, and

enhancing the accessibility to food products (Shahbazi & Jäger, 2020). Among the 3D food printing processes focused on biomaterials, extrusion-based printing is regularly applied to the extrusion of hot-melt chocolate (Mantihal, Prakash, Godoi, & Bhandari, 2017), cookie dough (Pulatsu, Su, Lin, & Lin, 2020), meat puree (Lipton et al., 2010), and processed cheese (Shahbazi, Jäger, & Ettelaie, 2021a, 2021b).

In the 3D extrusion printing, the bio-based polymeric inks need to be prepared such that shear-thinning, viscoelastic, and thixotropic behaviors are obtained to improve the ink multi-functionalities upon the 3D printing process. The printable inks must easily flow through a nozzle tip, and should also possess enough mechanical strength to develop well-

* Corresponding author. University of Natural Resources and Life Sciences, Vienna Department of Food Science and Technology, Institute of Food Technology, Muthgasse 18, 1190 Wien, Austria.

** Corresponding author. University of Natural Resources and Life Sciences, Vienna Department of Food Science and Technology, Institute of Food Technology, Muthgasse 18, 1190 Wien, Austria.

E-mail addresses: shahbazim00@yahoo.com, m.shahbazi1366@gmail.com (M. Shahbazi), henry.jaeger@boku.ac.at (H. Jäger).

<https://doi.org/10.1016/j.foodhyd.2021.107054>

Received 2 March 2021; Received in revised form 12 July 2021; Accepted 20 July 2021

Available online 22 July 2021

0268-005X/© 2021 The Author(s). Published by Elsevier Ltd. This is an open access article under the CC BY license (<http://creativecommons.org/licenses/by/4.0/>).

defined geometries. The supramolecular polymers largely affect the rheological features of ink-based dispersion, even when present at relatively low concentrations (Mantihal et al., 2017; Shahbazi & Jäger, 2020). However, the printable inks containing unmodified biopolymers suffer from poor flow behavior, low structural strength, and weak printing performance. The surface-active biopolymers, in contrast, are an important additive in the production of an effective emulsion-based system in terms of emulsion stability and flow properties. They are also efficient steric stabilizers thanks to their high molecular weight and the presence of numerous active binding groups for adsorption at hydrophobic-hydrophilic interfaces. A suitable biopolymeric surfactant for the emulsion stabilization must offer satisfactory interfacial activity and should interact with the oil phase to avoid emulsion instability. In this sense, the biosurfactants participate effectively in emulsion stability against coalescence/flocculation, in which the thickness of the adsorbed interfacial layer is sufficient to offer stability through the provision of steric repulsions and/or interaction of hydrophilic/hydrophobic domains of biosurfactant with the comparable groups in these systems (Kokubun, Ratcliffe, & Williams, 2015). Thus, introducing a surface-active biopolymer possibly enhances the manufacturing speed of printable ink-based emulsions, developing the desired 3D printed structure through strengthening the interlayer adhesion amongst the deposited layers.

The non-printable fibrous-based structure like meat needs the modification of its matrix by different crosslinking methods to obtain an extrudable paste-like component with desired printability and stability of 3D structures. Although several studies reveal the assessment of different methodologies and foodstuffs to 3D printed meat with diverse properties, one of the biggest challenges is still achieving the desirable textural features (Bohrer, 2019). On the other hand, policymakers and industries related to sustainable manufacturing have an outlook towards shifting consumer's attitudes to consuming more sustainable products. The meat analogue industry has made great steps over the past few years, and is anticipated to attain a value of \$21.23 billion worldwide by 2025 (Bohrer, 2019). Estimates specify that the market will pursue to develop such products and that the meat analogues will improve in terms of their formulation, nutritional application, and sensory perception. Plant-based meat substitutes are established to meet the customer requirements and sustainability of the forthcoming future food supply and the marketplace has progressively been developed over the last few years. Though some progress has been established to assemble the plant-based resources functionally similar to an animal-sourced protein, it remains a challenge to reproduce the hierarchical structure of meat tissue known to contribute to the general sensory properties of meat. The plant-based meat analogues should be sustainable products with functional characteristics and sensory properties (*i.e.*, appearance, texture, and flavor) similar to animal meat. In this sense, 3D printing allows the fabrication of healthy and sustainable food systems with acceptable sensory attributes and offers end-users, custom-designed, and personalized products with innovative experiences in taste and feel (Lipton et al., 2010; Sun, Peng, Yan, Fuh, & Hong, 2015).

Based on our findings reported in Part I of the present study (Shahbazi, Jäger, Ettelaie & Chen, 2021c), the optimum parameters to achieve the superior formulation to fabricate the reduced-fat soy-based inks were determined. In this sense, the produced emulsion gels based on using ethyl (hydroxyethyl) cellulose (oil to EHEC ratio 40:60 %) and dodeceny succinylated inulin (oil to DS inulin ratio 20:80 %) were shown to be optimum printable ink in terms of their shear-thinning behavior, viscoelastic properties, and thixotropic character with a monomodal particle size involving relatively small particles, followed by those on formulating with octenyl succinic anhydride (oil to OSA starch ratio 40:60 %) and acetylated (oil to acetylated starch ratio 40:60 %) starches. It was concluded that the inks exhibiting strong *pseudo-plastic* characteristics, coupled with desirable viscoelastic behavior and possessing reversible recoverable networks, might be more easily extruded from the nozzle, while providing enough mechanical strength

to resist deformation after their deposition.

Our initial hypothesis was based on the fact that reduced-fat soy-based emulsion gels that include surface-active biopolymers can be easily shaped in a three-dimensional fashion upon printing, providing stable structures with suitable mechanical properties. The technique applied in this study was the 3D printing process based on a laboratory-based additive layer manufacture, which offers rapid prototyping and can print soy-based ink into 3D structures that offer quality attributes to the end-products. In this context, the soy-based emulsion gels with different kinds of biosurfactants were formulated to produce a certain number of objects via the 3D printing technique. The effects of different biosurfactant types on the printing performance, textural properties, thermal behaviors, crystalline patterns, morphological features, and oral tribology of 3D printed constructs were explored. Given the dynamic profile of oral processing, the current work has also contributed by considering the temporality of sensations upon mastication through temporal dominance of sensations (TDS), where the results of the TDS score were compared with the findings of instrumental analysis methods.

2. Methods and materials

2.1. Materials

Materials were introduced and characterized in detail in the earlier publication (Shahbazi, Jäger, Ettelaie, & Chen, 2021c). Briefly, soy protein isolate (SPI) was purchased from Archer Daniels Midland Company (ADM, Decatur, IL). The FXL inulin with an average DP ≥ 23 was provided from Cosucra (Warcoing, Belgium) and modified using (2-dodecen-1-yl)succinic anhydride to yield hydrophobically modified inulin (Kiumarsi, Majchrzak, Yeganehzad, Jäger, & Shahbazi, 2020). The ethyl (hydroxyethyl) cellulose (EHEC) with an average molecular weight of about $100,000 \text{ g mol}^{-1}$, degree of ethyl substitution ($DS_{\text{ethyl}} \approx 0.8$), and molar degree of hydroxyethyl substitution ($MSEO \approx 2.1$) was supplied from Akzo Nobel Surface Chemistry AB (Stenungsund, Sweden). Acetylated wheat starch (DM-239) with an amylose/amylopectin ratio of 23:77 and substitution degree of 1.8 was purchased from Dongguan Dongmei Food Co., Ltd (Guangdong, China). Octenyl succinic anhydride (OSA) starch was supplied from National Starch Food Innovation (Hamburg, Germany). Sodium dodecyl sulfate (SDS), Bradford reagent, 1,4-dithiothreitol (DTT), Urea, monopotassium phosphate, dipotassium phosphate, and dithiothreitol were all obtained from Sigma (Sigma-Aldrich GmbH, Sternheim, Germany). Canola oil and salt were purchased from the local market. Beet juice extract was obtained from Nature's Bounty (Winnipeg, Manitoba, Canada). The Big Fry Burger® (BFB) as commercial plant-based meat was purchased from a local market (Fry's Family Food, UK). The BFB was considered for the comparison of textural and tribological behavior with the developed 3D printed samples in the current study. Its main ingredients included vegetable protein (soy and wheat gluten), sunflower seed oil, corn flour, methylcellulose, and salt. All other reagents used were analytical grade without further purification.

2.2. Preparation of soy protein-based ink

The soy protein-based inks were produced through the replacement of canola oil by surface-active biopolymers as stated in Part I of this series of work (Shahbazi et al., 2021c). The SPI aqueous dispersion was developed by dispersing about 40 g SPI powder into the part of the deionized water, with the rest of the water being used to disperse the surface-active biopolymers. Next, salt (0.1 g) and beet juice extract as a colorant (0.3 % v/v) were introduced into the SPI-based dispersion and stirred at 35 °C for 120 min with a magnetic heater-stirrer. At the same time, 10 % (v/v) canola oil was dispersed in the SPI-based solution using a burette and mixed with an Ultra-Turrax device (IKA* T25 digital, Germany) at 56 s^{-1} (367 G-force) for 5 min. Separately, the

biopolymeric surfactants were individually incorporated into deionized water with a level of 4 g/100 g (biosurfactant/water) and stirred at 50 °C for 120 min.

The biosurfactant dispersions were separately added to the coarse SPI-based emulsion to partially or totally replace its oil and heated at 35 °C with stirring for 120 min. These coarse ink-based emulsions were subsequently homogenized at room temperature through a Microfluidizer processor (M110-PS, Microfluidics international Corp., Newton, MA) at 5 MPa for two cycles. The stabilized emulsion containing 10 % (v/v) canola oil, regarded as control hereafter (40 wt% SPI, pH 5.40) was used to produce reduced-fat emulsion gels (Shahbazi et al., 2021c). The soy protein-based inks produced from EHEC, OSA starch, acetylated starch, and dodecyl succinylated (DS) inulin were coded as MAC, MAO, MAA, and MAI, respectively. All printable inks were conditioned in a controlled bio-chamber (ACS Sunrise 700 V, Alava Ingenieros, Madrid, Spain) at 25 °C with a relative humidity of (45 ± 2)% for 48 h prior analysis.

2.3. Printing process

The 3D printing process of soy protein-based ink was performed using a cold extrusion-based system (Mycusini®, Procusini, Freising, Germany), which is suitable for the fabrication of 3D printed food objectives with different shapes and geometries. With the use of computer-aided design software (AutoCAD; Autodesk Inc., San Rafael, CA), heart, cylindrical, and star-shaped meat analogues were modeled and converted to an STL file. These geometrical designs allowed the simple evaluation of the printing performance and construct quality features (shape reliability, edge aspect, material layering) among 3D printed object variants. The print paths were provided through the creation of the G-code files to control XYZ direction instruction of the printer, developed by the open-source CAM software Slic3r (slic3r.org, consulted on September 2020) from the STL file. The Slic3r software is a 3D slicing engine to translate virtual 3D models into printing instructions aimed at the printing process. The prepared printable ink-based emulsions were carefully put into the stainless-steel cartridge with a volume of 10 mL. The filled cartridge was stirred through a Vortex mixer (Fisher Scientific, Ontario, Canada) for 10 min to eliminate the air bubbles trapped in the ink. To assess the influence of the surface-active biopolymers on the printing performance, the printing settings were adjusted according to different preliminary trials. The layer height was set at 1 mm, proposing that the nozzle tip was elevated by that same value upon completion of the fabrication of each layer. The layer deposition processes were continued until the suitable 3D architectures were printed. The height of the tip was increased by 1.1 mm after the deposition of each layer. The number of deposited layers was 20 and the width of the tip was 1 mm. Table 1 summarizes the settings used to investigate the printing performance of the soy protein-based inks. The

Table 1
The printing settings are expressed as Slic3r terms (<http://slic3r.com>).

Printing adjusting	Sign	Value	Units	Definition
Nozzle diameter	D	1.0	mm	Nozzle diameter
Layer height	Z	1.0	mm	Layer height
Extrusion flow speed	Q	0.40	mL min ⁻¹	Continuous extrusion flow rate provided by the syringe pump
Flow rate	S	90	%	The volume of ink that passes through the extruder
Infill velocity	V	15	mm s ⁻¹	Spindle speed during extrusion
Travel velocity	V _{travel}	180	mm s ⁻¹	The spindle speed of a jump between the end of one extrusion and the next
Perimeter	P	10	–	Number of outline layers
Infill density	ρ _{infill}	90	%	Quantity of material filling the object

fabricated 3D printed architectures were initially conditioned at an RH of (84.3 ± 2)% with a saturated solution of KCl at 25 °C for 2 days. Their final moisture content was equilibrated at a level of (59.5 ± 1.4)%. After conditioning, the 3D printed constructs were enclosed within a specific aluminum specimen box and stored at 4 °C to prevent dehydration.

2.4. Characterization of 3D printed meat analogues

2.4.1. Printing performance

The printing performance of different 3D printed architectures, as affected by different formulations, was evaluated. Each printed construct was placed into a specific chamber (20 cm × 20 cm × 20 cm) aimed at taking photos. The photos were captured through a digital camera (Alpha 7M3 E-Mount, Full-Frame Mirrorless, 24.2 MP, Sony, Tokyo, Japan). Three replicates of each printed architecture were assessed by measuring line width and layer number using a digital caliper (Mitutoyo, Absolute Digimatic, Tokyo, Japan) (Shahbazi et al., 2021b).

2.4.2. Textural properties

Textural parameters of the 3D printed meat analogues and the commercial meat analogue were considered. These included the sample hardness, cohesiveness, gumminess, springiness, and chewiness, inferred from the force-deformation curves obtained using a texture analyzer (TA.XT-plus, Stable Micro Systems, Godalming, UK), as based on the TPA method. Eight 3D printed objects were cut as cylindrical shape (30 mm × 30 mm) and then were compressed with a cylindrical probe (75 mm diameter). The speed of compression was set at 5 mm s⁻¹, with a compression distance of 8 cm and a peak force limit of 15 N. The maximum force encountered during the process was considered as the sample hardness. The cohesiveness was determined by the proportion of the positive force zone upon the second compression step during the first compression phase. The gumminess was obtained by multiplying hardness and cohesiveness measured values. Springiness was considered as the height recovered during the period between the completion of the initial compression and the start of the second compression. The chewiness was measured as gumminess × springiness. All TPA variables were analyzed via the Exponent Lite software (v.6.1.4) (Majzoubi, Shahbazi, Farahnaky, Rezvani, & Schleining, 2013).

2.4.3. Protein solubility assay

The protein solubility of the 3D printed constructs was performed with different extracting solvents as reported by Chen, Wei, & Zhang

Table 2
A summary of extracting solutions with selecting reagents and their mixtures applied for evaluating protein solubility.

Serial number	Extracting solution	Definition
1	Phosphate buffer (PB); 0.1 M phosphate buffer consisting of KH ₂ PO ₄ and K ₂ HPO ₄ with a pH of 7.5	Native state protein
2	PB + Urea (PU); 8M urea	Hydrogen bonds
3	PB + DTT (PBD); 0.05 M dithiothreitol	Disulfide bonds
4	PB + SDS (PBS); 1.5 g/100 mL sodium dodecyl sulfate	Hydrophobic interactions
5	PB + U + DTT (PBUD)	Interactions between hydrogen bonds and disulfide bonds
6	PB + U + SDS (PBUS)	Interactions between hydrogen bonds and hydrophobic interactions
7	PB + DTT + SDS (PBDS)	Interactions between disulfide bonds and disulfide bonds
8	PB + U + DTT + SDS (PBUDS)	Interactions among hydrogen bonds, disulfide bonds, and hydrophobic interactions

(2011) and Chiang, Loveday, Hardacre, and Parker (2019) with some modifications. Table 2 summarizes extracting solution variants to identify the particular chemical bonds within 3D printed structures. These extracting solutions solubilize the protein through the degradation of diverse kinds of intermolecular chemical linkages (Chen, Wei, & Zhang, 2011). A tiny amount of 3D printed samples was dispersed in each extracting solution (10 g L^{-1}) and stirred using a magnetic stirrer for 120 min at the ambient temperature. Then, the dispersion was sheared using a high-speed rotor-stator device (Ultra-Turrax, IKA* T25 digital, Germany) for 20 min. The process generated shear forces at a shear rate of 210 s^{-1} (5690 G-force). Next, the sheared dispersions were passed through a two-stage high-pressure Microfluidizer processor (M110-PS, Microfluidics international Corp., Newton, MA) with a pressure of 80 bar at the first stage and 30 bar at the second stage. Afterward, the supernatant was carefully filtered through in-line filtration (Millipore Millex-HV PVDF, $0.45 \mu\text{m}$) and was collected. The concentration of soluble proteins in the supernatants was measured by the Bradford protein measurement using a spectrophotometer which recorded the absorbance at a wavelength of 595 nm with a multi-plate reader (Biotek, Winooski, VT).

In this regard, bovine serum albumin powder was considered as the standard. The total nitrogen in the original samples was measured using the Kjeldahl method (Owusu-Apenten, 2002). The protein content was measured through a conversion factor of 6.25. The protein solubility was obtained as the proportion of soluble protein in the supernatant to total protein in the 3D printed objects.

2.4.4. Thermal measurement

The thermal behavior of 3D printed objects, as affected by bio-surfactant types, was assessed through a differential scanning calorimeter (DSC) (DSC-Q100, TA Instruments, New Castle, DE). A tiny amount (approximately 5 mg) of 3D printed samples were located on an aluminum pan and afterward heated from $-60 \text{ }^\circ\text{C}$ to $180 \text{ }^\circ\text{C}$ at a heating rate of $10 \text{ }^\circ\text{C min}^{-1}$, under an oxygen-free nitrogen flow rate of 40 mL min^{-1} . The thermal variables, including glass-transition temperature (T_g), melting peak (T_m), and peak enthalpy were automatically calculated through the TA Data Analysis software (TA Instruments, New Castle, DE). The T_g was defined as the mid-point temperature of a step-down transition in the baseline that resulted from the discontinuity of the specific heat. The T_m was considered as the temperature at which the heat capacity of the endothermic peak reached the maximum rate (Shahbazi, Majzoobi, & Farahnaky, 2018a).

2.4.5. Morphology structure

The influences of different types of surface-active biopolymers on the morphological structure of the 3D printed objects were captured through a variable-pressure scanning electron microscope (VP-SEM Quanta 200 FEG SEM, FEI Company, Eindhoven, Netherlands) to produce high-resolution images with a high-depth of field. Initially, each 3D construct was cut into a precise size of $(15 \times 15 \times 15) \text{ mm}^3$. Next, the sectioned 3D printed samples were mounted on a Peltier-cooled stage with a temperature of $-10 \text{ }^\circ\text{C}$ to avoid thermal damage. The nitrous oxide was utilized as an imaging gas that offered a pressure of 50.7 Pa. The microstructures of each 3D construct were obtained through a solid-state backscatter detector via an accelerating voltage of 20 kV.

2.4.6. Crystallography

An X-ray diffraction (XRD) technique, to analyze the crystalline pattern of 3D printed meat analogue, was employed here using an XRD instrument (Philips X-Pert PRO, Netherlands). The experiment was conducted with the energy of 40 kV, 30 mA current, and Cu $K\alpha$ irradiation ($\lambda = 1.54056 \text{ \AA}$). The 3D constructs were irradiated in the range of $3\text{--}50^\circ$ and scanned with a speed of $0.018^\circ \text{ min}^{-1}$ at room temperature. To evaluate the relative crystallinity degree (RCD), total curve area (I_t)

and the area under the peaks (I_p) were measured through the software offered with X'pert Highscore Plus (v2.0, PANalytical, The Netherlands). This allows for RCD to be calculated from Eq. (1) (Shahbazi, Majzoobi, & Farahnaky, 2018b):

$$\text{RCD (\%)} = (I_p/I_t) \times 100 \quad (1)$$

2.4.7. Oral tribology measurements

Saliva is an important compound of oral lubrication and must be introduced in a tribological experiment aimed at a desired simulate of the in vivo circumstances. The unstimulated whole saliva (4 mL) was collected based on established work by Navazesh, 1993 with some modification. In short, ten non-smoker participants (5 males and 5 females) were instructed to refrain from eating or drinking (excluding water) for 2 h before the saliva collection in the morning (10 a.m.). The panelists were then requested to rinse their mouth with drinking water four times and subsequently the saliva produced by chewing a silicone cube (35 mm diameter) was collected. The participant placed the cube in their mouth with 5 mL of water and chewed for about 20 s before expectorating. Finally, they were asked to continue chewing for a further 2 min while collecting saliva in a 50 mL centrifuge tube served in ice. Approximately, 4 mM imidazole/acetate buffer (pH 7.0) was added to the freshly collected saliva (1:1 v/v) and centrifuged (Beckman, GS-15R Palo Alto, CA) at 2000 G-force for 5 min. The imidazole/acetate buffer (pH 7.0) was further incorporated into the supernatant to dilute it to 16 (v/v)% of the unstimulated whole human saliva for the tribological analyses. This was stored at $-18 \text{ }^\circ\text{C}$ for further tests.

To evaluate the lubricant properties of the 3D printed objects and also the commercial meat analogue, oral tribology measurements of saliva (*ex vivo*) were conducted using a ring-on-plate tribo-rheometry (TA Instrument, New Castle, DE). This involved a rough hydrophobic surface of 3M Transpore Surgical Tape 1527-2 (3M Health Care, St Paul, Min), which was considered as the state with a comparable surface roughness ($R_a = 31.5 \mu\text{m}$) and wettability to the human tongue (Nguyen, Nguyen, Bhandari, & Prakash, 2016). A half-ring rheometry was utilized to provide the refill of material between the two solid surfaces. The tape was cut in a square form, located, and compacted tightly on top of the lower plate rheometry. After each experiment, the tape was changed and the tribo-rheometry was cleaned and dried with deionized water and laboratory wipes. The extent of 3D printed samples was sufficient to cover the surface of the substrate offered by the thin film. To mimic the sensory process, the normal forces of 2 N were used to denote the adequate normal force employed upon typical oral processing (Miller & Watkin, 1996). Moreover, the oral condition was simulated at a temperature of $37 \text{ }^\circ\text{C}$. All 3D printed samples were pre-sheared at a speed of 0.01 s^{-1} for 2 min and were equilibrated for a further 1 min before each experiment. The human tongue has been estimated to move at speed up to 200 mm s^{-1} (Hiemae & Palmer, 2003), with the tribology experiment conducted in this work falling in this desired range. Afterward, the rotational speed was ramped from 0.01 to 200 mm s^{-1} , with the attainment of 25 measured points per decade. During the tribological test, the coefficient of friction (CoF) was determined as the ratio of friction stress (σ_F) to the normal stress (σ_N), described by Eq. (2):

$$\text{CoF} = \sigma_F/\sigma_N = (M/F_N) \times [(r_2 + r_1)/(r_2^2 + r_1^2)] \quad (2)$$

where, M is torque (Nm) and F_N is normal force (N), r_1 is inner ring (14.5 mm) and r_2 is the outer ring (16 mm) radii.

Moreover, the coefficient of friction could be plotted versus the increasing sliding speed, defined as follows:

$$\nu_s = \bar{R} \times \omega \quad (3)$$

Here, ν_s is the sliding speed (mm s^{-1}), \bar{R} is the mean value of the inner and outer ring radii, and ω is the controlled rotational speed (rad s^{-1}).

2.5. Temporal dominance of sensations (TDS)

2.5.1. Selection of terms and panel instruction and training

Ten assessors (five females and five males, aged: 24–34 years) participated in this study. They were designated to evaluate the dynamic sensory experiment based on the guidelines of the ISO 8586 standard (ISO, 2012) and were familiarized with the sensation of meat analogue products. Two 1-h preliminary sessions were conducted to define the TDS methodology and the notion of the temporality of sensations, offering the participants the chance to investigate the data collection software and become acquainted with it. The most frequently mentioned sensory features were selected and their descriptions and procedure to evaluate them were developed. The selected attributes for 3D printed meat-analogue objects were listed as firmness, juiciness, oiliness, graininess, dryness, fibrousness, chewiness, fattiness aftertaste, and residue aftertaste. Each attribute reference, applied to acquaint the panelists, is shown in Table A-1 in Supplementary Materials. The assessors were afterward trained to employ the computerized TDS data capture system (FIZZ v 2.40A) according to the procedure defined by Pineau et al. (2009). The assessors were required to place the sample into their mouth first and click on the start button to begin the assessment. At 15 s, they were asked to swallow the printed objects via a message presented on the screen and continue the assessment once no attribute was perceived. Then, the assessors were instructed to click the stop button, except data acquisition had automatically stopped upon the time of 60 s. Afterward, the evaluators were requested to identify the sensory attributes they had perceived as being dominant during the testing procedure. Evaluators were informed that they did not have to choose all the attributes in the list and that they could select a similar sensation many times during the assessment or to never choose a descriptor as being dominant.

2.5.2. Formal assessment

The temporal dominance of sensations (TDS) method was employed to express variances in the dynamic sensory profile of 3D printed meat analogue variants. The TDS evaluation was performed over two sessions to run two replications. The 3D printed objects (3 cm × 3 cm) were provided to the assessors by randomized complete block design in a monadic order (one-at-a-time). The panelists were then presented with a list of nine attributes on the computer screen, each associated with an unstructured scale anchored from weak to strong. To obtain a sensory property of the evolving dominant attributes at the panel level, the normalized time was plotted versus the dominance rate or selection frequency of each trait at a specified point in time (%). Each curve displayed the progress of the dominance rate of an attribute over time (Pineau et al., 2009). In this sense, FIZZ software (Version 1.9, Biosystems, Counternon, France) was utilized to obtain the TDS plots, where two lines were displayed on each TDS graph, namely chance- and significance levels to simplify the interpretation of attributes. The TDS plots were smoothed by MATLAB software (R2016a, MathWorks Inc., Natick, Ma) for a better presentation. The chance level signifies the minimum magnitude of a dominance rate that a trait was attained by chance ($1 \times (\text{number of attributes})^{-1}$). The significance level states the least magnitude of a dominance rate of a given trait, which is significantly higher than the chance level ($P < 0.05$) (Pineau et al., 2009). The TDS score was also measured as average intensity scores weighted by the duration of each selected sensation during the assessment. Besides, the TDS score was measured as the mean of the score related to a specific trait during an assessment weighted by their duration. The TDS score for each sensation was measured as follows:

$$\text{TDS score} = (\sum_{\text{scoring}} \text{Intensity} \times \text{Duration}) / (\sum_{\text{scoring}} \text{Duration}) \quad (4)$$

2.6. Statistical analysis

All instrumental experiments were carried out as triplicate determinations (except textural properties, where eight replications were used). In all cases, the mean and standard deviation of the data were reported. Analysis of variance (ANOVA) was utilized for the determination of the main effects of the examined independent factors and their interactions on the instrumental and sensory data. Duncan's multiple range test was applied to separate means of data when significant differences ($P < 0.05$) were observed. Principal component analysis (PCA) was conducted through Unscrambler (Version 9.2, CAMO A/S, Oslo, Norway) to identify or distinguish the clusters in a data population to visualize the main variation in the data with the principal components (PCs). The obtained score plot, where all objects are plotted according to the new coordinates from the transformed data, allows for easy identification of the main differences in the data set, with clustering of the samples frequently becoming obvious using the first few PCs. A corresponding plot of variables, the correlation loading plot, shows the correlations between the different variables.

3. Results and discussion

3.1. Printing performance

The instrumental findings in Part I of this study (Shahbazi et al., 2021c) demonstrated that the coded soy protein-based inks of MAC-60 (40:60 % oil to EHEC ratio), MAI-80 (20:80 % oil to DS inulin ratio), MAO-60 (40:60 % oil to OSA starch ratio), and MAA-60 (40:60 % oil to acetylated starch ratio) showed a higher degree of stability against droplet coalescence/flocculation, a greater level of *pseudoplasticity*, a higher structural strength, and resulted in the formation of strong gel-like networks when compared to the rest of formulations in Part I of this series (Shahbazi et al., 2021c). Moreover, the matrices encountered in these inks were found to be thixotropic, with the restoration of their initial structures upon removal of stress/deformation. Then, these printable inks were considered to be suitable candidates for the 3D printing process and worthy of further investigation. Fig. 1 illustrates different 3D printed meat analogue architectures constructed by consecutive printing of layers, as prepared by several different bio-surfactants variants. Moreover, Table 3 summarizes the collected data regarding the layer number and line width, which correlate with the structural strength and printing accuracy, respectively (Liu, Zhang, Bhandari, & Yang, 2018). All the printable soy protein-based inks containing surface-active biopolymers could easily be extruded out from the nozzle tip. This was not entirely surprising; because they showed strong *pseudoplasticity* (Shahbazi et al., 2021c). In the reduced-fat emulsion gels, there were enough amphiphilic groups in the system for hydrophobic and hydrophilic interactions, sufficient to contribute to the formation of a strong gel-like network (*i.e.*, higher elastic modulus, enhanced yield stress, and greater viscosity recovery with the strong thixotropic feature). These 3D printed reduced-fat architectures could withstand applied extrusion shear forces and allowed for a high level of dimensional resolution in an appropriate end-product shape, with several built-up layers. However, the printed control objects deformed in time due to sagging (after 2 min), and subsequently displayed poor resolution and weak shape-fidelity as found for different shapes including star, heart, and cylindrical-shaped objects (Fig. 1). A less shear-thinning character of control ink, as reflected by the higher flow index behavior compared to other ink varieties, means the rising difficulty in the extrusion process (Shahbazi et al., 2021b). A large yield stress (as the minimum force required for extrusion), a high elastic modulus, coupled with low creep recovery compliance, representing the mechanical strength of a printable ink, are essential features to support

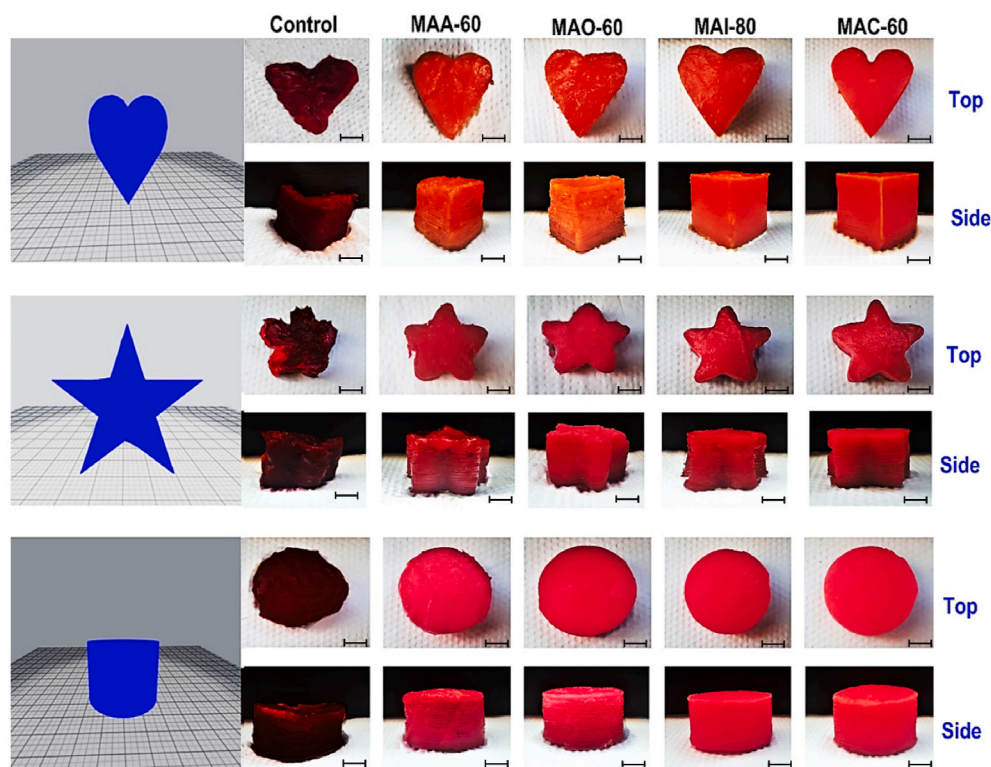


Fig. 1. The heart, star, and cylindrical-shaped 3D printed reduced-fat meat analogue architectures prepared using different biosurfactants. For better clarification, the color channel for each designed shape was slightly altered. The scale bar is 2 cm. (For interpretation of the references to color in this figure legend, the reader is referred to the Web version of this article.)

Table 3
Line widths and layer numbers of 3D printed meat analogues variants.

Sample	Heart		Cylindrical		Star	
	Line width (mm)	Layer numbers	Line width (mm)	Layer numbers	Line width (mm)	Layer numbers
Control	2.12 ± 0.06 ^d	7 ± 2 ^a	2.44 ± 0.08 ^c	6 ± 2 ^a	2.02 ± 0.05 ^c	6 ± 2 ^a
MAC-60	1.13 ± 0.02 ^a	17 ± 1 ^c	1.41 ± 0.01 ^a	16 ± 1 ^c	1.15 ± 0.03 ^a	17 ± 2 ^c
MAI-80	1.41 ± 0.03 ^b	16 ± 1 ^c	1.30 ± 0.04 ^a	17 ± 1 ^c	1.32 ± 0.01 ^b	16 ± 1 ^c
MAO-60	1.70 ± 0.03 ^c	13 ± 1 ^b	1.76 ± 0.04 ^b	12 ± 1 ^b	1.56 ± 0.01 ^c	13 ± 1 ^b
MAA-60	1.73 ± 0.04 ^c	13 ± 1 ^b	1.78 ± 0.02 ^b	13 ± 2 ^b	1.62 ± 0.01 ^d	12 ± 2 ^b

^{a-e} Means inside each column with different letters are significantly different ($P < 0.05$), Duncan's test.

the deposited layers and preserve the 3D printed shape (Shahbazi & Jäger, 2020; Shahbazi, Jäger, Ahmadi, & Lacroix, 2020). In this sense, the control ink with an inferior yield stress, weak elastic gel-like structure, and modest thixotropic features did not offer a structured network system (Shahbazi et al., 2021c), thus resulting in low precision geometries and poor spatial resolution, as was observed in the control architectures.

As captured in Fig. 1, certain alterations happened within the 3D printed geometries, formulated with various biosurfactants. It was also found that the 3D printed MAC-60 and MAI-80 structures matched well with the designed 3D model in their length or width and height, showing the finest resolution and a smooth surface, providing the desired appearance. This was expected since these ink counterparts exhibited more shear-thinning, an enhanced yield point, stronger elastic behavior, and low creep compliance (Shahbazi et al., 2021c). These functional features offered the 3D printed architectures a better shape retention capability and stable structural properties. It was reported that the highly desirable inks for 3D printing purposes possess enhanced *pseudoplastic*, viscoelastic, and thixotropic features, with a reversible restructuring that can simply be extruded out from a nozzle tip and is capable of preserving the 3D printed shapes (Godoi, Prakash, &

Bhandari, 2016; Dankar, Pujolà, El Omar, Sepulcre, & Haddarah, 2018). Moreover, smaller droplets that are regularly distributed in the ink system could offer reduced-fat inks to enhance mechanical stability upon printing (Shahbazi et al., 2021b). Among the printed reduced-fat meat analogues, the printed MAO-60 and MAA-60 showed a somewhat inferior printing performance and dimensional stability. These also caused some extension of the line-edge roughness, in contrast to structures printed using MAC-60 and MAI-80. According to the intrinsic viscosity and molecular weight results, reported in Part I of this series (Shahbazi et al., 2021c), there was a lack of sufficient biopolymeric chains in OSA and acetylated starches in the confined system, for chain entanglement and chain-chain interactions to occur, particularly when compared with EHEC and DS inulin. This led to the formation of a gel-like network that was rather weak and could not support the following deposited layers. This resulted in wider line width and a smaller number of layers, together with a slight level of deformation or collapse. The inferior performance can also be attributed to a lower viscosity recovery, decreased yield stress, as well as a smaller elastic modulus, provided by OSA and acetylated starches in comparison to EHEC and DS inulin, which could somewhat reduce the printing accuracy and spatial resolution.

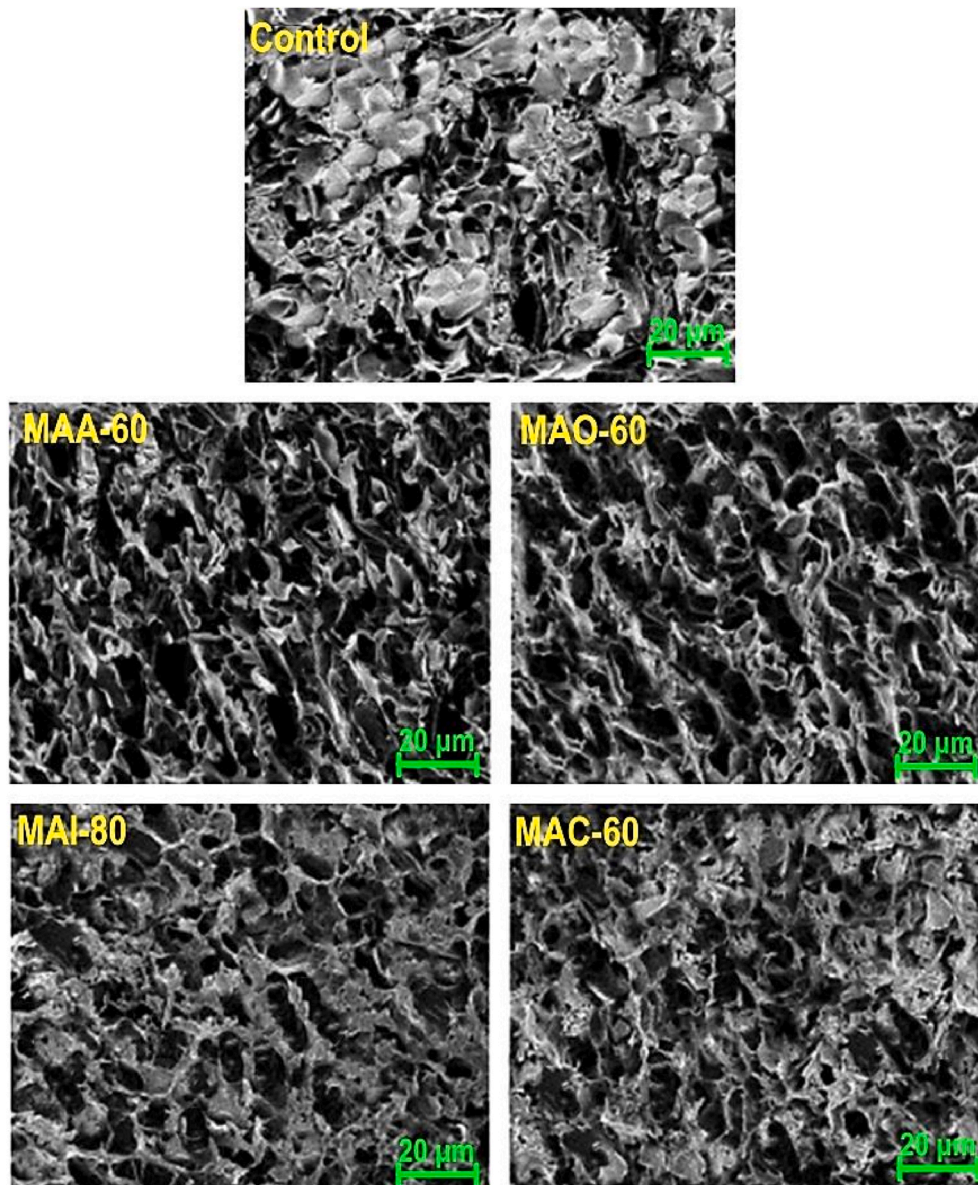


Fig. 2. VP-SEM photomicrographs of meat analogues fabricated using various ink formulations, involving different types of biosurfactants.

3.2. Microstructure of 3D printed meat analogues

To evaluate the effect of different types of biosurfactants on the morphology of printed SPI-based meat analogue, a VP-SEM assay was performed on the surface of the 3D structure. The microstructures of the 3D printed meat analogue formulated with biosurfactant variants are displayed in Fig. 2. As visualized, the surface morphology of the 3D printed control object was characterized by some level of irregularity and the presence of aggregated micro-sized lumps on the surface. There was also minimal interlayer spacing. This uneven and heterogeneous structure could be attributed to the lack of biopolymeric surfactant in the production of 3D printed control construct. In contrast, a high level of porosity, with the uniform structure in terms of orientation and shape of spaces, was observed in the objects printed using reduced-fat meat analogue containing biosurfactants. The micrographs also revealed a high solid packing density, with fewer void spaces for printed MAC-60 and MAI-80 as compared to those printed using MAO-60 and MAA-60. This indicates a slightly denser matrix. In these cases, a strong interaction between hydrophilic and hydrophobic domains of EHEC and DS

inulin with comparable groups of SPI and oil, respectively, led to the formation of a more compact structure. These results were in agreement with those for a strong gel-like network, higher viscosity recovery, and lower creep compliance of emulsion gels (Shahbazi et al., 2021c). Once again, they demonstrated that the utilization of biosurfactants in the 3D printing process of meat analogue could positively affect the microstructure. A porous 3D structure can affect the printing performance and dimensional stability of the printed object (Shahbazi et al., 2021b). Additionally, the VP-SEM micrographs detected the interconnected networks with a highly porous structure for printed MAO-60 and MAA-60. However, as mentioned earlier, these had slightly lower packed matrices and a less dense structure compared to printed MAC-60 and MAI-80. When comparing the thick wall of 3D printed meat analogue perceived from micrographs, a markedly thicker wall was observed for the printed MAC-60 and MAI-80. In contrast, a relatively larger pore size distribution and the thinner wall were obtained for the printed MAO-60 and MAA-60 samples. This was consistent with the results obtained for the printing performance.

3.3. Textural features

Textural properties can offer valuable information about 3D printed foods since they are strongly associated with the final quality of food products. Several methods have been used to investigate the textural parameters of a plant-based meat formulation. These include measurement of force and deformation at the point of rupture upon stretching of extrudates (Osen, Toelstede, Wild, Eisner, & Schweiggert-Weisz, 2014), texture evaluation by shearing (Thiébaud, Dumay, & Chefel, 1996), and compression force analysis (Lin, Huff, & Hsieh, 2000). The textural parameters of 3D printed meat analogues variants and the commercial meat analogue (BFB), obtained by TPA, are summarized in Table 4. The force required to compress the 3D constructs during the first bite represents the sample hardness. As can be seen, the hardness of the 3D printed control was lower than those of the printed reduced-fat meat analogues, while the BFB was detected to be the hardest sample. The lower level of hardness of the 3D printed control could be explained by the weaker structural strength of this ink. In turn, this is characterized by the lower elastic modulus, inferior yield stress, and poor stability to permanent deformation (Shahbazi et al., 2021c). Compared to the 3D printed control, the level of hardness was significantly increased when meat analogue was formulated using EHEC, DS inulin, OSA starch, and acetylated starch ($P < 0.05$) (Table 4). The fact that the reduced-fat inks were characterized by a high elastic modulus and low creep compliance indicated the formation of a strong gel-like network in these printed reduced-fat constructs (Shahbazi et al., 2021c). Among the 3D printed objects, printed MAC-60 presented a remarkably higher degree of hardness than the other samples, followed by MAI-80. This could possibly be due to the lower critical overlap concentration, a higher intrinsic viscosity, and a greater molecular weight of EHEC and DS inulin (Shahbazi et al., 2021c). Moreover, the thicker wall of printed MAC-60 and MAI-80, detected by VP-SEM, could offer the formation of a denser structure. This then led to the promotion of the 3D architectures, with reinforced mechanical strengths. The printed MAO-60 and MAA-60 had identical hardness values ($P > 0.05$) (Table 4), which might be ascribed to the similarities between their ink counterparts in terms of their rheological and thixotropic behavior (Shahbazi et al., 2021c).

Cohesiveness is an indicator of the structural strength of internal linkages, which maintains the 3D printed matrix together in a bolus and prevents it from decomposing into fragments upon swallowing. As shown in Table 4, a noticeable increase in the cohesiveness was detected when biosurfactants were used in the formulation of meat analogue. This change was possibly once again related to the development of a well-defined gel-like network structure in the reduced-fat inks, promoted by the presence of surface-active biopolymers (Shahbazi et al., 2021c). The 3D printed MAA-60 and MAO-80 presented higher cohesiveness values among the printed reduced-fat constructs. The TPA data

also showed that BFB offered the greatest cohesiveness value (Table 4). Gumminess denotes the magnitude of work required to make an object ready to swallow, and once again, the printed MAA-60 and MAO-80 presented notably higher levels of gumminess as compared to the rest of the printed samples. As is clearly shown in Table 4, once again BFB exhibited the highest gumminess value. Compared to the printed control, the gumminess values were increased by 121.7, 122.9, 145.5, and 147.3 % for printed MAC-60, MAI-80, MAO-60, and MAA-60, respectively. The greater value of gumminess obtained for biopolymeric surfactants may be the result of these promoting a denser matrix and a reversible network in the reduced-fat ink formulations (Shahbazi et al., 2021c).

Springiness, also referred to as elasticity, can be considered as the rubbery properties of a material in the mouth. It is an amount of how much the material structure is broken down by the initial compression. From Table 4, a higher springiness value for the printed reduced-fat constructs was detected compared to the printed control ($P < 0.05$). In this context, the springiness value of the printed MAC-60 and MAI-80 were greater than the printed MAA-60 and MAO-80. This observation agreed well with the results of creep recovery reported in Part I of this series of studies (Shahbazi et al., 2021c), where the MAC-60 and MAI-80 inks offered greater relative creep recoveries, and consequently also higher elasticities. The TPA data also exposed that the chewiness parameter was similarly higher in the meat analogues containing the surface-active biopolymers. The chewiness of the 3D printed MAC-60 and MAI-80 both showed greater values when compared to the printed MAO-60 and MAA-60 objects. It is interesting to note that the highest value of the chewiness parameter was detected in the BFB (Table 4).

When the instrumental TPA parameters for each 3D printed construct are considered collectively, the printed MAC-60 with its higher hardness, chewiness, and springiness showed a firm 3D structure. It is concluded that this structure needs more energy for initiation of the structural breakdown, but would simply fragment into pieces once the intermolecular linkages are degraded, because of its lower cohesiveness value (Sharma, Kristo, Corredig, & Duizer, 2017). The printed MAI-80 shares similarities with the printed MAC-60 when exposed to large deformations. Therefore, the high value of the structural strength of the 3D printed MAC-60 and MAI-80 can be translated into greater energy required to make a swallowable bolus. Compared to printed MAC-60 and MAI-80, the printed MAO-60 and MAA-60 objects displayed a weaker structure, presenting a lower level of hardness and chewiness. Nonetheless, these latter samples behaved quite opposite when considering gumminess and cohesiveness, having a higher degree of both cohesiveness and gumminess. This specifies that printed MAO-60 and MAA-60 constructs are likely to produce a swallow-able bolus more easily (Sharma et al., 2017).

Table 4
Summary of mechanical strength and thermal parameters of 3D printed constructs.

Sample	TPA parameters				Chewiness (N mm)	Thermal parameters				
	Hardness (N)	Cohesiveness	Gumminess (N)	Springiness (mm)		T _{g1} (° C)	T _{g2} (° C)	T _{g3} (° C)	T _{m1} (° C)	T _{m2} (° C)
Control	10.1 ± 0.3 ^a	0.32 ± 0.01 ^a	3.23 ± 0.21 ^a	2.5 ± 0.1 ^a	8.08 ± 0.32 ^a	-48.1 ± 0.4	-25.7 ± 0.1	-6.42 ± 0.02 ^a	59.5 ± 0.2 ^a	119.4 ± 1.1 ^a
MAA-60	12.1 ± 0.4 ^b	0.66 ± 0.03 ^c	7.99 ± 0.34 ^c	5.7 ± 0.1 ^b	45.54 ± 0.71 ^b	nd	nd	-0.44 ± 0.01 ^b	67.2 ± 0.1 ^b	133.6 ± 1.3 ^b
MAO-60	12.2 ± 0.3 ^b	0.65 ± 0.03 ^c	7.93 ± 0.32 ^c	5.8 ± 0.2 ^b	45.99 ± 0.66 ^b	nd	nd	-0.42 ± 0.02 ^b	68.1 ± 0.3 ^c	134.2 ± 1.5 ^b
MAI-80	15.0 ± 0.2 ^c	0.48 ± 0.03 ^b	7.20 ± 0.13 ^b	6.7 ± 0.3 ^c	48.24 ± 1.1 ^c	nd	nd	3.11 ± 0.04 ^c	68.0 ± 0.5 ^c	134.6 ± 1.3 ^b
MAC-60	15.9 ± 0.2 ^d	0.45 ± 0.02 ^b	7.16 ± 0.12 ^b	6.8 ± 0.2 ^c	48.69 ± 1.3 ^c	nd*	nd	3.93 ± 0.02 ^d	67.8 ± 0.3 ^c	134.8 ± 2.1 ^b
BFB	19.6 ± 0.3 ^e	0.75 ± 0.03 ^d	14.70 ± 0.34 ^d	6.7 ± 0.1 ^c	98.49 ± 2.1 ^d	-	-	-	-	-

^{a-e} Means inside each column with different letters are significantly different ($P < 0.05$), Duncan's test.

*nd: not detected.

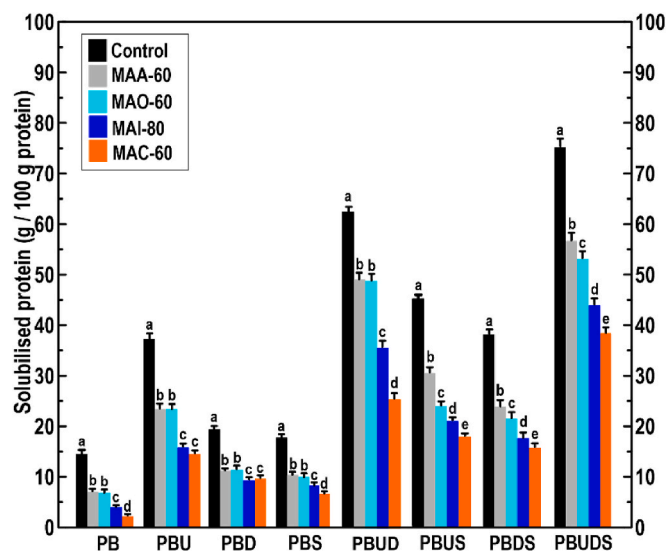


Fig. 3. Protein solubility values of 3D printed meat analogues as seen in different extracting solutions. The means inside each group, labeled with letters (a–e), are significantly different from each other ($P < 0.05$), Duncan's test.

3.4. Protein solubility of 3D printed objects in different extracting solutions

One important property of high moisture meat analogues is the fibrousness that resembles muscle meat. The protein solubility values of 3D printed constructs prepared by biosurfactants variants (with a moisture content of about 59.5 %) are shown in Fig. 3. The protein solubility, as solubilized by eight different extracting solutions, was measured by determining the dissolved protein levels obtained from different 3D printed architectures. As Fig. 3 depicts, the phosphate buffer (PB) extracted the minimum extent of protein from the 3D printed samples. This indicates the variety and the strength of intermolecular linkages in the meat analogues. In this respect, the printed MAC-60 showed the lowest PB extractability, followed by the printed MAI-80 sample. The results illustrate that these printed objects are more structured than those of printed MAA-60 and MAO-60 (Liu & Hsieh, 2007). On the contrary, the amount of solubilized protein for the 3D printed objects increased when Urea, DTT, or SDS were mixed with PB, *i.e.*, PBU, PBD, and PBS solvents, respectively. This is not surprising, as the protein molecules aggregate through more than one type of physiochemical bond (Lin et al., 2000). The values of protein solubilized using PBU were higher than those of PBD and PBS, demonstrating that hydrogen bonds were more important in the formation of the protein networks. Moreover, a lower solubilized protein value by PBS and PBD showed that the hydrophobic interactions and disulfide bonds were of less significance.

On the other hand, increasing DTT-solubilized protein for 3D printed MAC-60 and MAI-80 structures could suggest that disulfide bonds may have a role in the development of fibrous structure in these samples (Chiang et al., 2019). The protein solubility data also showed that the protein solubilized by a mixture of PBDS was somewhat comparable to that one solubilized by PBU. Moreover, when a multicomponent extracting solution was produced with PB, the magnitude of the solubilized protein from the printed meat analogues showed a greater increase. In this regard, the levels of the solubilized protein were found to be greatest for the two-component PBU solvents (*i.e.*, PBUD and PBUDS), reinforcing the fact that a high amount of protein was associated with hydrogen bond linkages. Compared to the sum of PBU and PBD, the protein solubility was higher with 3D printed objects placed in PBUD. This could be understood on the account of the synergistic effect of the two reagents. Liu & Hsieh (2007) stated a comparable synergy between Urea and DTT. On the other hand, the protein solubilized value was the

highest in the PBUDS mixture. This supports the fact that the structure of the 3D printed objects was formed and supported by a combination of hydrogen bonds, disulfide bonds, hydrophobic interactions, and their combinations. This shows the addition of biosurfactants promoting these bonds, and hence the formation of the protein fibrous structure.

3.5. Thermal behavior

The printing precision and construct stability are critical features for the fabrication of an appealing 3D printed architecture, and taking thermal behavior as an instance, melting temperature and glass-transition temperature provide valuable information on the suitability of a formulation in the printing processing. The DSC thermograms of different 3D printed meat analogues are shown in Fig. 4 and the data are summarized in Table 4. Heating can change soy protein structure from its native state to a denatured form, which can be seen as endothermic behaviors in DSC thermograms. Two distinguished endothermic peaks, detected in thermograms of the 3D printed control meat analogue, are likely due to the denaturation of the two main protein components of soybean protein, *i.e.*, the 7S (59.5 °C) and the 11S (119.4 °C) (Guerrero, Retegi, Gabilondo, & De la Caba, 2010). This indicates that an important fraction of the SPI remains in its native conformation as a globular structure, once subjected to the 3D printing process. Fig. 4 also shows that the peak enthalpies (ΔH) of the printed MAO-60 and MAA-60 were slightly decreased as compared to control. This is the result of some limited degree of denaturation in the protein structure. In comparison, the enthalpy of endothermic denaturation peaks was reduced far more for the printed MAI-80 and MAC-60 meat analogues, indicating this time a high level of protein denaturation and conformational changes. This denotes the development of a certain degree of interaction between functional groups of EHEC and DS inulin with SPI, associated with the disruption of intramolecular bonds in crystalline regions, thereby increasing the extent of semi-crystalline and/or amorphous areas (Guerrero et al., 2010). The alteration in the denaturation enthalpies of all the printed reduced-fat objects could also be associated with the changes in the bonding patterns, where a protein conformational structure with fewer or weaker bonds would require a lower amount of energy to unfold, as a consequence, a reduction in the enthalpy was observed (Guerrero et al., 2010). Also shown in Fig. 4, the manufacture of the 3D printed reduced-fat meat analogues, containing surface-active biopolymers, caused a considerable shift in the melting temperature (T_m) (transition temperature) of the denaturation peaks to the higher temperatures. This behavior is likely due to the presence of the hydrophobic/hydrophilic groups grafted to the backbone of the biopolymeric structures, causing the promotion of more structured and stable systems. In this context, the grafted ethyl (hydroxyethyl), dodecyl succinate, OSA, and acetate groups of the EHEC, DS inulin, OSA starch, and acetylated starch, respectively, could interact with oil. On the other hand, the polar biopolymer chain-end groups interact more favorably with the hydrophilic groups of SPI. This induces the formation of a more stable structure, which needs a greater temperature for disorganization and structural disordering.

The glass-transition behavior (T_g) of the 3D printed constructs was detected as the mid-point temperature of a step-down shift in baseline, on account of the discontinuity of the specific heat (Shahbazi et al., 2018a). The T_g is an important parameter related to the system mobility, considered as a physical change from a glassy to a rubbery state promoted by heat, in the amorphous materials. The DSC results revealed that there were three glass-transition behaviors in the printed control meat analogue, corresponding to oil-rich (T_{g1}), protein-rich (T_{g2}), and protein-water domains (T_{g3}). The first region, which is somewhat obvious from Fig. 4, is called T_{g1} ; according to the research studies is the starting of the T_{g2} area (Chen, Zhang, & Cao, 2005; Shahbazi, Ahmadi, Seif, & Rajabzadeh, 2016). The extents of T_{g3} , T_{g2} , and T_{g1} for the printed control construct were determined to be around -48.1 , -25.7 , and -6.4 °C, respectively. The 3D printed reduced-fat meat analogues

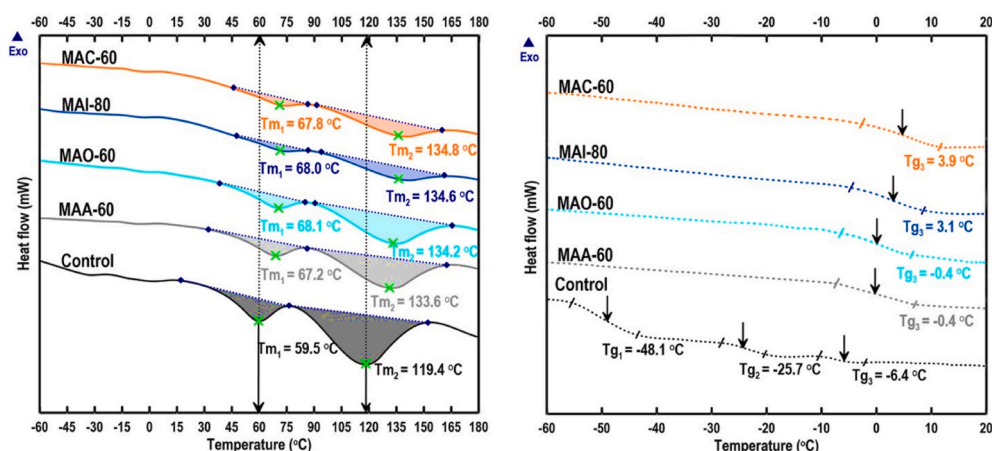


Fig. 4. The DSC thermograms of meat analogue variants (left) and their glass-transition behaviors (right). The heating rate is $10\text{ }^{\circ}\text{C min}^{-1}$.

containing surface-active biopolymers exhibited a single glass-transition behavior (T_{g3}). The result implies the existence of a homogeneous network structure (Fig. 4). This can be explained by the fact that the biopolymeric surfactants were compatible with SPI, suggesting a good level of miscibility between the components. Moreover, it can be seen that the glass-transition (*i.e.*, T_{g3}) of all the 3D printed meat analogues was moved to higher temperatures when compared to the printed control. This suggests the movement of chain segments was hindered after the inclusion of biosurfactant, which reflects in an increase in the glass-transition temperature (Guerrero et al., 2010). A shift in the T_g to higher temperatures is attributed to the development of a more stable structure, preventing motion of the polymeric chains, which then consequently need a higher temperature for the structural disorganization. The T_g (*i.e.*, T_{g3}) values of the 3D printed MAO-60 and MAA-60 were increased by $6\text{ }^{\circ}\text{C}$ compared to the printed control, which is noticeably less than the printed MAC-60 and MAI-80. This to some extent can be attributable to interactions between functional groups of OSA or acetate starches with oil and SPI, showing an impact on the structural mobility, even when present at a small mass fraction. The T_g values of printed MAC-60 and MAI-80 showed a greater increase by $10.3\text{ }^{\circ}\text{C}$ and $9.5\text{ }^{\circ}\text{C}$, respectively. A huge hindrance in the movement of polymeric chain segments caused by EHEC and DS inulin might be the result of more than sufficient interactions between functional groups of surface-active biopolymers and the SPI/oil system. Moreover, a denser matrix and the thicker walls of the 3D printed MAC-60 and MAI-80, as illustrated by the VP-SEM micrograph, indicate a likely decrease in the polymer mobility. This result is in accord with the rheological and structural investigations carried out for soy protein-based inks involving EHEC and DS inulin, as was reported in Part I of this series of studies (Shahbazi et al., 2021c).

3.6. Crystalline pattern

The XRD experiment was utilized to further prove the impact of surface-active biopolymers on the structural reorganization and crystalline pattern of the 3D printed meat analogue (Fig. 5). The obtained X-ray diffractogram of the printed control object showed a strong reflection at a 2θ value of about 14.8° and a distinct peak at a 2θ value of $\sim 21^{\circ}$. It was reported that the peak angles of α -helix and β -sheet structures raised from soy proteins appear at around $2\theta = 10^{\circ}$ and $2\theta = 20^{\circ}$, respectively (Chen et al., 2013; Zhao et al., 2015). Soy proteins contain the non-polar and polar amino acid residues, which induce strong inter- and intramolecular interactions, including hydrogen bonding, charge-charge, dipole-dipole, hydrophobic interactions, etc. The strong ionic and polar interactions amongst the polymeric side chains hamper the segmental rotation and molecular mobility within the matrix. This leads to some degree of local ordering of SPI (Guerrero

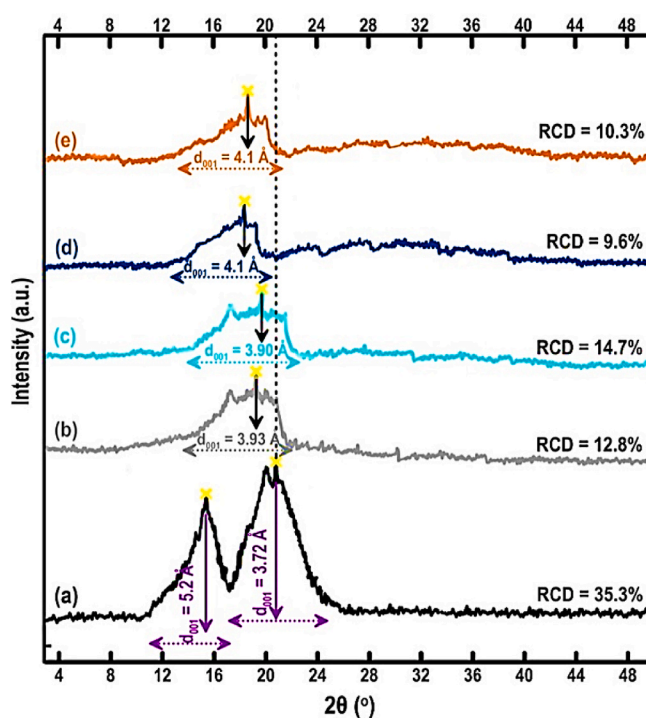


Fig. 5. The XRD patterns of 3D printed meat analogue variants. (a): printed control, (b): printed MAA-60, (c): printed MAO-60, (d): printed MAI-80, (e): printed MAC-60. RCD represents the relative degree of crystallinity.

et al., 2010). In the current study, the presence of oil in the 3D printed control slightly reduced the relative crystallinity degree (RCD) of soy protein isolate from 36.1 % to 35.3 % (data not shown); suggesting the development of printed SPI/oil did not change the basic local ordering of SPI. Compared to printed control, the diffractograms of printed reduced-fat meat analogue variants showed a noticeable change in the structural reorganization pattern and local ordering. This evolution could be, at least partially, explained by the transformation and redistribution of the basic crystal lattice (local ordering) within the matrix. The XRD patterns of 3D printed MAO-60 and MAA-60 showed the conversion of the characteristic peaks by losing α -helix and a reduction in the peak of β -sheet structure, attributed to a decrease of ϵ -amino groups upon interacting with OSA and acetate starches (Li et al., 2015). In this regard, the RCD dramatically dropped to about 12.8 % and 14.7 % for printed MAA-60 and MAO-60, respectively. These results are supported by the DSC findings, in which the interaction between

functional groups of modified starches and SPI residues could decrease the local ordering of SPI in the meat analogue matrix. Likewise, the XRD pattern of the printed MAI-80 was characterized by a reduction in the *RCD* to 9.6 %, inferred from the total disappearance of the distinct peak at $2\theta = 14.8^\circ$ and a notable decrease in the peak area of β -sheet. These correspond to a decrease of α -helix and an increase of disordered coils. As presented in Fig. 5, the diffractogram of the printed MAC-60 was also characterized by the loss of α -helix peak at $2\theta = 14.8^\circ$ and a decreased peak intensity of β -sheet. The *RCD* also decreased to 10.3 %. This implies a decrease in the intensity of local ordering and the disappearance of the main SPI diffraction peaks. In this sense, the active hydroxyl/carboxyl groups on the biopolymeric backbone acted as a hydrophilic point, while the grafted ethyl (hydroxyethyl) and dodecanyl succinylate groups define the hydrophobic edges, giving the printed reduced-fat meat analogues an overall amphiphilic character. This leads to the increased multiple binding sites at the interface, inducing structural reorganization with a disordered arrangement. There are several investigations in the literature attributed to decreasing the relative crystallinity degree after incorporation of modified hydrocolloids (Li et al., 2015).

The average distance between layers (interlayer d_{001} spacing) for the printed control were determined to be $d_{001} = 5.2 \text{ \AA}$ ($2\theta = 14.8^\circ$) and $d_{001} = 3.7 \text{ \AA}$ ($2\theta = \sim 21^\circ$). Regarding 3D printed reduced-fat meat analogues fabricated by OSA and acetate starches, the pronounced peak of the β -sheet structure slightly shifted to the lower 2θ values, which specified that d_{001} spacing (gallery spacing) from $d_{001} = 3.7 \text{ \AA}$ ($2\theta = \sim 21^\circ$) increased to $d_{001} = \sim 3.9 \text{ \AA}$ ($2\theta = \sim 19^\circ$). The shift to the lower angle indicates an increase in the corresponding interlayer spacing, which means that the components have a less ordered structure (Guinier, 1994). This result indicated that the interaction of functional groups of modified starches by SPI resulted in changes in the spatial structure and unfolding of protein molecules, decreasing the chain mobility. The greatest shift to the lower 2θ values was detected in the printed MAC-60 and MAI-80, coinciding with an increase in gallery spacing to $d_{001} = 4.1$

\AA ($2\theta = \sim 18$), indicating a hindrance in chain segment motion with a huge redistribution of the basic crystal lattice. In this regard, the polar groups of biosurfactants could strongly interact through hydrogen bonding between $-\text{OH}$ (in threonine, tyrosine, and serine), $-\text{COOH}$ (in glutamic acid), $-\text{NH}_2$ (in lysine and arginine), $-\text{NH}-$ (in histidine and proline) groups, and peptide bonds in the SPI. This reduces inter- and intramolecular interactions among protein chains, and therefore dis-ordering of polymeric chains, and consequently decreased local ordering of SPI (Guerrero et al., 2010).

3.7. Oral tribology properties

Tribology refers to the lubrication feature of two interacting surfaces once they are in relative motion. Oral tribology relates to understanding the interaction of food with saliva-coated oral surfaces. The Stribeck curve is frequently employed to describe the lubrication feature by plotting the coefficient of friction of the lubricant against the sliding speed (Chen & Stokes, 2012). The Stribeck curves ($\log \text{CoF}$ versus $\log \nu_s$) of the 3D printed meat analogue variants and the commercial meat analogue are depicted in Fig. 6a and the resulting friction coefficient is illustrated in Fig. 6b. As Fig. 6a depicted, all 3D printed meat analogues presented both boundary and mixed regimes of typical Stribeck curves. The friction performance results also showed that the lubrication behavior of 3D printed samples did not change at the sliding speeds of $< 1 \text{ mm s}^{-1}$ (Fig. 6a). At this low sliding speed ($0.01 \leq \nu_s \leq 1 \text{ mm s}^{-1}$), known as the boundary regime, there is not enough lubricant that enters or remains in between the two surfaces. The friction behavior in the boundary regime is mainly governed by the properties of the contacting surfaces, such as surface roughness rather than the viscosity of the lubricant (Chen, 2009).

Beyond boundary regime ($\nu_s \geq 1 \text{ mm s}^{-1}$), known as the mixed regime, more lubricant is entrained into the contact offering improved surface separation. At this point, the lubricant develops a thin

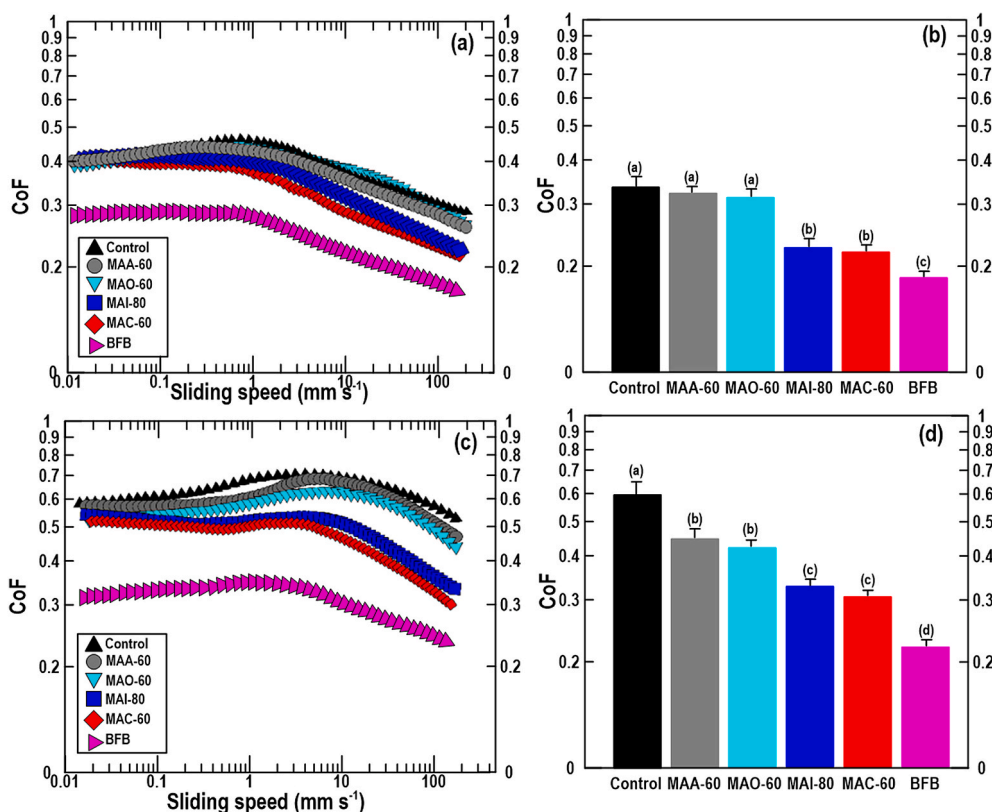


Fig. 6. The friction curves of meat analogues variants without (a) and with saliva (c). The obtained friction coefficient of meat analogues without (b) and with saliva (d). The means inside each column with different letters (a–d) are significantly different ($P < 0.05$), Duncan's test.

continuous film able to partially support the load, which leads to the decreased friction effects (Czichos, 2009). The friction coefficients measured in the mixed regime could be considered for understanding the material behavior in the oral processing, texture, and mouthfeel (Chen & Stokes, 2012). In the mixed regime, the friction coefficients mainly depend on functional features of both the surfaces and the lubricant, as well as the interactions between the lubricant and surfaces. Fig. 6a illustrates the lubrication behavior of 3D printed meat analogues was notably changed in the mixed regime. Compared to printed MAA-60 and MAO-60, the *CoF* was significantly decreased regarding printed MAI-80 and MAC-60 ($P < 0.05$) (Fig. 6b), which is an indication of the desired lubrication behavior. As mentioned, the reduction in friction is principally governed by the flow properties and molecular-level

interaction that promote fluid entrainment. Then, the observed changes between 3D printed meat analogues in the mixed area could partly be ascribed to the higher elastic modulus and the development of a strong gel-like network in the ink systems formulated by modified inulin and modified cellulose (Shahbazi et al., 2021c). As reported in Part I of this series (Shahbazi et al., 2021c), compared to OSA and acetate starches, the EHEC and DS inulin showed a higher value of intrinsic viscosity with a greater molecular weight, which exerted a substantial effect on the structural strength of soy-based ink.

An important aspect of the oral tribology of solid and semi-solid foods is the application of saliva to produce a swallowable food bolus. Saliva affects the lubrication behavior and the existence of saliva in the oral environment could then alter texture perception of the food

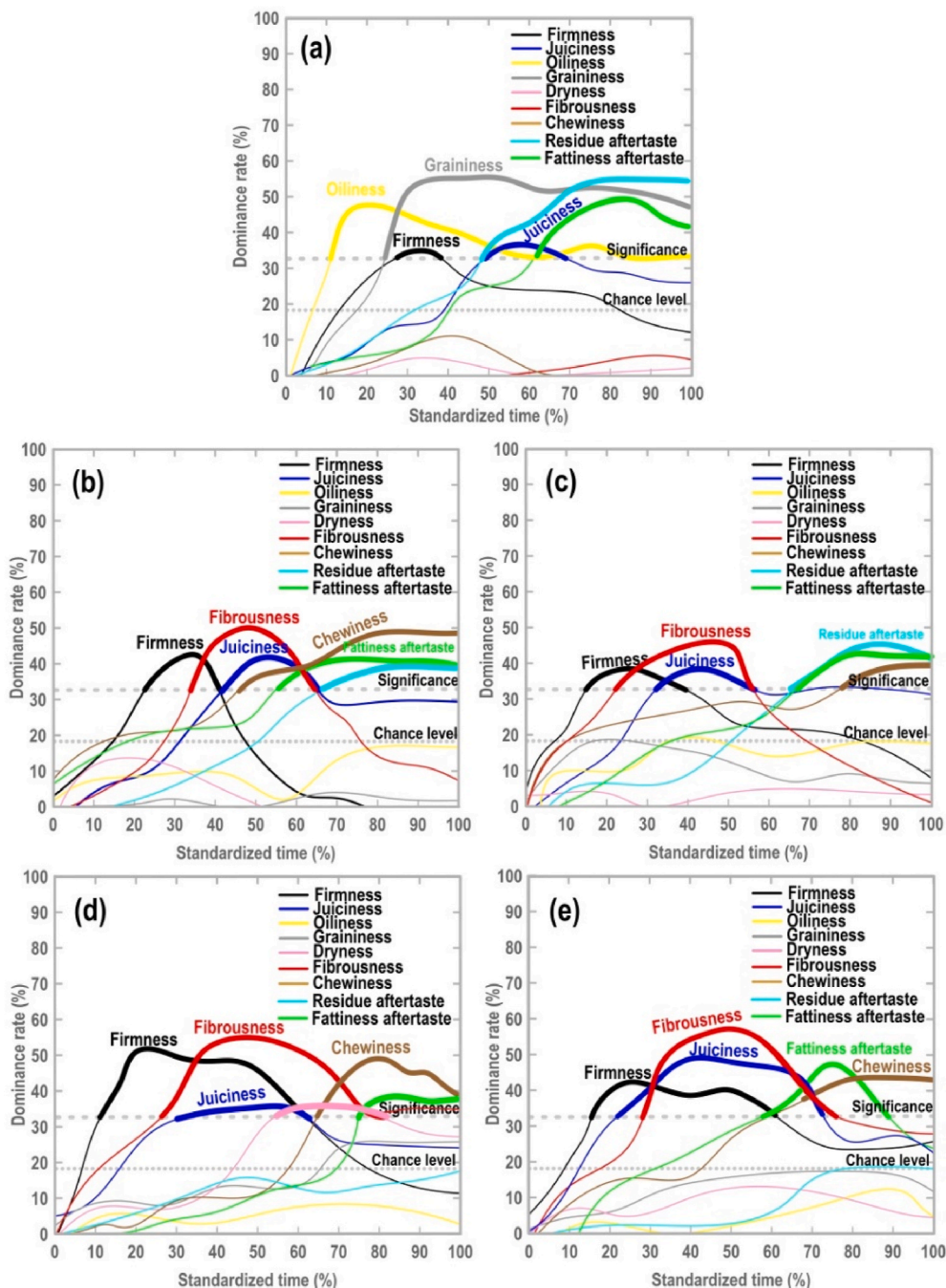


Fig. 7. Temporal profiles of dominant sensations in standardized time with specific attributes in meat analogue samples. (a): printed control, (b): printed MAA-60, (c): printed MAO-60, (d): printed MAI-80, (e): printed MAC-60.

products (Czichos, 2009; Chen & Stokes, 2012). The tongue in the dry form has a hydrophobic character. In the presence of saliva, the tongue shows more hydrophilic features as a result of the adherence of amphiphilic proteins existing in saliva. Therefore, it was expected the saliva lubricates the hydrophobic 3M Transpore Surgical Tape surface pretty well. Unexpectedly, the lubrication behavior of 3D printed meat analogues exposed the saliva-containing samples offered higher *CoF* (Fig. 6c and d) compared to those of free-saliva ones (Fig. 6a and b). The tribological results showed that when saliva-containing 3D printed meat analogues were sheared between the evaluated hydrophobic surfaces, there was an increase in the *CoF* compared to 3D printed samples without saliva. This result is strange as saliva behaves as a brilliant lubricant, reducing wear through developing a resistant layer made of salivary proteins (Chen, 2009). In this scenario, saliva apparently acted like a bulk protein concerning adherence and increasing the *CoF*. Another reason for such behavior could be assigned to the dilution effect of the 3D printed samples with saliva. Dilution decreases the rheological properties, which leads to a higher value of *CoF*. As a consequence, adherence of proteins from either 3D printed meat analogue, saliva, or both, as well as the dilution effect principally increased the *CoF*.

3.8. Dynamic sensory evaluation

The sensory properties of 3D printed products are crucial features determining their acceptance by consumers. In this context, temporal sensory procedure considers being important to truly understand consumer's attitudes and their hedonic responses. TDS is a method established to attain temporal information for numerous descriptors upon product consumption (Pineau et al., 2009). The smoothed TDS curves with the respective TDS chance and significance levels are shown in Fig. 7. Each TDS curve shows the sensory profile of the 3D printed meat analogue variants related to the evaluated attributes during the standard time of 100 %. Based on the binomial distribution and considering 30 observations, the chance level (18 %) and the significance level (32 %) were obtained and plotted over TDS curves to the assessment of the sensory data. In the temporal profiles of 3D printed reduced-fat constructs, firmness, fibrousness or juiciness, and chewiness or fattiness aftertaste were perceived as a dominant attribute at the beginning, middle, and the end of mastication, respectively. The oiliness was only dominant in the printed control at the beginning of the evaluation, from a standardized time of about 10 %, and dominated nearly throughout the entire evaluation period with a maximum dominance rate (max. *DR* %) of 47.5 %. Moreover, textural attributes of juiciness (max. *DR* = 35.7 %) also exceeded the significance level for the printed control between the standardized time of about 48–69 % of the evaluation period. The role of oil in meat analogue formulation is to contribute to the juiciness, tenderness, and fatty/oily feeling of the product (Szczesniak, 2002). Moreover, the temporal profile of printed control was distinguished from the other 3D printed reduced-fat samples with graininess, where this attribute significantly dominated at the middle of the evaluating period with max. *DR* of 53.7 % and dominated during the entire evaluation period ($P < 0.05$). This was consistent with the fact that the printed control was characterized by some levels of heterogeneity and the presence of aggregated micro-sized lumps on its surface as shown by VP-SEM. Furthermore, the temporal profile of printed control was dominated by fattiness aftertaste (max. *DR* = 47.6 %) in addition to the dominance of residue aftertaste (max. *DR* = 52.2 %) mainly at the end of mastication. Compared to 3D printed reduced-fat meat analogues, printed control was formulated with the highest oil level (i.e., 10 % (v/v)), which could explain the fattiness aftertaste trait during the mastication process. Regarding 3D printed reduced-fat objects, the residue aftertaste in the printed MAO-60 (max. *DR* = 37.2 %) and MAA-60 (max. *DR* = 44.9 %) was also marked as dominant by the panelist at the end of mastication, albeit with lower dominance rates in comparison with printed control. Similarly, TDS profiles of printed MAO-60 and MAA-60 showed the fattiness aftertaste was less dominated compared to

printed control likely due to the lesser amount of oil component. In the case of printed MAC-60 and MAI-80, the panelists were also able to perceive the fattiness aftertaste as a dominant attribute with a max. *DR* of 36.4 % and 44.2 %, respectively, even with a reduced fat content, providing important information about the role of EHEC and DS inulin in the texture of the reduced-fat meat analogue.

The TDS curve of firmness demonstrated a similar trend in all 3D printed objects, increasing at the beginning of the evaluation and drastically decreasing around the middle of the standardized time. The printed control showed the lowest firmness attribute (max. *DR* = 33.8 %). This result is in accordance with the TPA test, where the printed control presented the lowest hardness value. As stated in Part I of this series (Shahbazi et al., 2021c), the control ink precursor showed poor viscosity value, weak elastic modulus, and high creep compliance with larger particle size resulted from the lack of surface-active biopolymers present at the produced O/W interface required for surface coverage (Shahbazi et al., 2021c). Compared to printed control, the printed reduced-fat meat analogues were dominated by firmness for a long time above the significance level and higher dominant rate, whose max. *DR* was determined to be 38.3 %, 43.1 %, 50.7 %, and 42.3 % regarding printed MAO-60, MAA-60, MAI-80, and MAC-60 respectively. The biopolymeric surfactants change the food texture allowing differences in sensory profiling, as detected in the present study. Earlier investigations have stated that modified starch offers a rigid texture to some solid foods (Ilhamto, 2012; Sharma et al., 2017). The modified inulin has also been reported could provide substantial firmness in some food products (Kiumarsi et al., 2019). The development of a strong gel-like network resulted from higher rheological and mechanical parameters, as shown in Part I of this series (Shahbazi et al., 2021c), could be contributed to a greater force required to chew the 3D printed reduced-fat objects. In this sense, the printed MAI-80 showed a firmer matrix with a higher max. *DR* and longer dominance time due to some extent higher structural strength, which could be translated into higher energy needed to make a swallow-able bolus. Similarly, the juiciness also exceeded the level of significance in the middle of the evaluation period in all the printed reduced-fat samples with greater dominance regarding MAC-60 (max. *DR* = 48.6 %). Additional promising results in the role of biopolymeric surfactants on the sensory feature of 3D printed meat analogue refer to the printed MAC-60 and MAI-80, which had a 60 % and 80 % oil reduction, respectively. Compared to printed MAO-60 and MAA-60, the printed MAC-60 and MAI-80 revealed greater dominance of fibrousness throughout the mastication period with a max. *DR* of 54.8 % and 55.2 %, respectively. These results were supported by the protein solubility in different extracting solutions, where the disulfide bonds became progressively important in the printed MAC-60 and MAI-80 as a sign of the development of the fibrous structure. By referring to earlier statements, the instrumental texture parameters of these printed objects were notably higher than those of printed MAO-60 and MAA-60. This proposes a denser network structure with strong 3D structural strength, leading to a development of a proper matrix.

On the other hand, graininess and dryness (except MAI-80) defects in the printed reduced-fat meat analogues were not perceived as significantly dominant at any time of evaluation ($P > 0.05$). This was consistent with the fact that the formation of a homogenous matrix with a uniform structure, smaller pore size distribution, and thinner wall cell with a highly porous structure (obtained by VP-SEM) upon the incorporation of surface-active biopolymers. Due to their matrices, the biopolymeric surfactants acted as an active filler and are known to promote a well-defined gel-like network structure and the stabilization of meat analogue emulsions. A long-lasting chewiness was also perceived significantly at the end of mastication, attaining the maximum dominance rate of *DR*% = 47.1 %, *DR*% = 38.4 %, *DR*% = 49.6 %, and *DR*% = 43.4 % regarding printed MAO-60, MAA-60, MAI-80, and MAC-60 respectively. In the case of printed MAI-80, dryness made a minor peak but a significant appearance at the middle of the consumption time with a max. *DR* of 34 %, which showed that the DS inulin provided a

slightly drier and rougher feeling texture, which affected the final texture perception of the printed sample. This might be supported by the fact that the lower oil content of printed MI-80 compared to the other reduced-fat meat analogue formulations.

3.9. Correlations of instrumental and sensory measurements

Interrelationships between defined sensory attributes and instrumental parameters will contribute to the formulation of accurate texture products with the consideration of complex expression differences in the dynamic sensory profile (Kiumarsi et al., 2021). PCA was performed to assess the correlations between the instrumental readings of printing performance, thermal parameters, relative crystallinity degree, tribology, and mechanical data and TDS score obtained from the dynamic sensory evaluation. This correlation can help to better understand the behavior of biosurfactants in the 3D printed reduced-fat meat analogue. The TDS score is an amount of sensory sensation intensity as mean intensity scores weighted by the duration of each selected sensation during the assessment. It was measured by Eq. (4) from the TDS data of each TDS attribute. The obtained score plot of printed meat analogue variants within each group is shown in Fig. 8, where the PC1 and PC2 described 59.7 % and 19.8 % of the variation in the data set, respectively. The 3D printed samples were separated into clusters associated with the meat analogue formulated with different biosurfactants. The printed MAC-60 and MAI-80 formed two clusters on the PC1 axis in the score plot compared to the other samples (Fig. 8a). The printed MAA-60 was also clustered on the left-hand side of the score plot, while printed MAO-60 was almost clustered in the center in the score plot among the printed MAA-60, MAC-60, and MAI-80 samples. Fig. 8b shows the corresponding loading plot of measured variables. The parameters placed nearby to each other show a positive correlation, whereas the ones with loadings of opposite signs are negatively correlated. This plot was affected by instrumental variables of printing performance, texture, thermal, tribological, crystalline parameters, where the results of layer numbers, hardness, gumminess, chewiness, d_{001} spacing, CoF , Tm_1 , and Tm_2 were placed close to each other to the right side of the plot, representing a high correlation among these variables. Moreover, the PC1 clearly distinguished these parameters as opposed to the peak enthalpies (ΔH_1 and ΔH_2), line width, two theta (2θ), and relative crystallinity degree (to the left). The corresponding loading plot was also affected by the TDS score, in which sensory assessments of firmness, fibrousness, juiciness, and chewiness were localized in the same area of the correlation loading (to the right), specifying a positive correlation. However, there was a negative correlation between these sensory attributes with perceived oiliness, graininess, and dryness.

To be of value, the sensory evaluation needs to be validated with instrumental measurements. The higher predictability of the instrumental readings with sensory studies translates into greater validity of instrumental characteristics. In this context, a correlation between instrumental parameters and TDS score obtained from the sensory evaluation was conducted (Fig. 8b). The positive correlations were obtained between TDS scores of firmness, juiciness, fibrousness, and chewiness and instrumental readings of layer numbers, d_{001} spacing hardness, gumminess, chewiness, CoF , Tm_1 , and Tm_2 , which supports the fact that the printed reduced-fat meat analogues would require a higher force necessary to chew the 3D structures. A research study in the earlier publication was stated the strong correlations among these instrumental texture measurements and oral firmness (Sharma et al., 2017). Hardness is the extent of strength/overall resistance of a 3D printed sample against deformation and gumminess is a measure of the energy required to produce a swallow-able bolus. A positive correlation of these parameters with chewiness and fibrousness indicates a firm sample will need more energy to deform. In contrast, graininess, dryness, and oiliness attributes correlated with the relative crystallinity degree and enthalpy of endothermic peaks and negatively with chewiness, hardness, and gumminess, indicating that graininess, dryness, and oiliness also provide a good estimate of instrumental textural parameters. Swallowing is related to the textural traits perceived upon early periods of oral processing, which varies with the type of surface-active biopolymers. It is then concluded the desired firmness, chewiness, and fibrousness sensations of 3D printed meat analogues with lower graininess, oiliness, and dryness descriptors requiring some level of energy to compress and produce an appropriate ready-to-swallow bolus, specifies the proper mixing with saliva, and therefore might offer the perception of sample juiciness.

4. Conclusions

This research was state-of-the-art knowledge and state-of-the-art technology to develop an innovative approach in the search of strategies for designing a 3D printed reduced-fat plant-based sample for a point-of-use meat analogue. This study provided a methodology to fabricate a fibrous 3D printed reduced-fat meat analogue with taking advantage of different types of surface-active biopolymers, which is particularly valuable; as clear differences between the meat analogues produced using similar methods and ingredients can be difficult to fabricate technologically satisfactory interfaces. This indicated that 3D printing techniques and biosurfactants can be combined to make a well-defined porous meat analogue with improving spatial resolution and fabricating personalized nutrition for customers. In this sense, this work

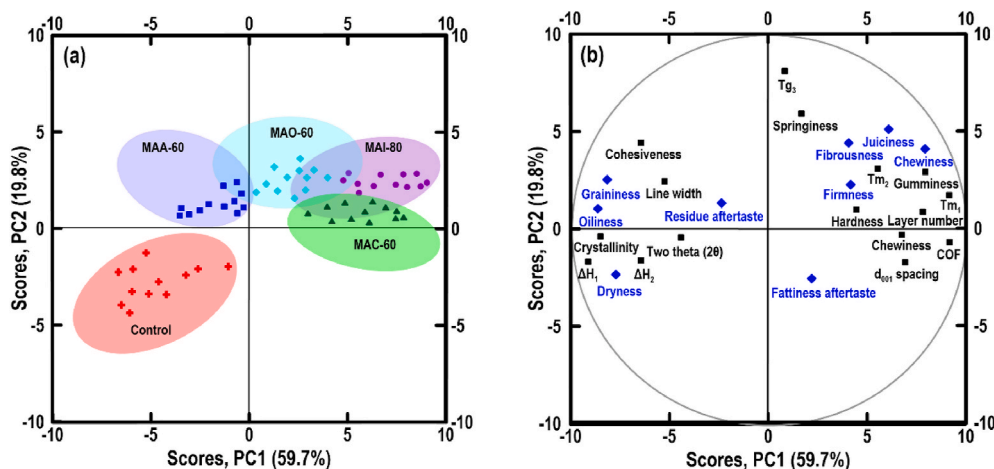


Fig. 8. PCA of the results from all 3D printed objects showing the first two principal components (PC1 and PC2). (a) Score plot showing all meat analogues within each group. (b) Correlation loading plot of the measured variables (♦ sensory attributes (TDS score), ■ instrumental measurements).

demonstrated the utilization of biopolymeric surfactant variants were key factors influencing the printing performance, microstructure, thermal, tribological, and structural features of 3D printed meat analogue. The incorporation of biosurfactant variants promoted the formation of protein anisotropic structures and improved the fibrous degree of the 3D printed structures. These outcomes may most particularly have implications in the fabrication of a fibrous reduced-fat meat analogue, with an approach valid for solid or semi-solid products in general. Oral tribology was shown to depend on biosurfactant variants where less deformable (firmer) printed samples decreased surface-surface contact and reduced friction coefficients, improving lubrication property. Given the in-mouth situations appropriate for the sensory perception, we also explored the effect of saliva on the lubrication, in which the mixing of 3D printed samples with saliva led to an increase in the friction coefficient compared to that one saliva-free product. One significant aspect of the current work was also based on dynamic sensory evaluation, presenting the texture of 3D printed meat analogues as perceived through oral processing differs with surface-active biopolymers variants. The surface-active biopolymers affected the texture of 3D printed meat analogue, giving differences in dynamic sensory perception. According to the dynamic sensory data, the replacement of oil by biopolymeric surfactants in the meat analogue is recommended to produce a fibrous 3D printed reduced-fat meat analogue, in which the printed reduced-fat constructs presented a desired sensory profile. The results could support a strategic methodology to minimize oil consumption in the meat analogue products with the utilization of biosurfactants, and subsequent application of 3D printing to improve resolution and shape-fidelity of 3D printed objects. This study offered fabrication of a well-defined 3D printed reduced-fat meat analogue, which their effectiveness and performance for the additive manufacturing and meat emulsion industry are promising.

Compliance with ethics requirements

The authors declare no conflict of interest.

Author statement

Mahdiyaz Shahbazi: Conceptualization, Methodology investigation, Collecting data, Validation, Data interpretation, Funding acquisition, Writing – Original draft, Writing – Review & Editing. Henry Jäger: Methodology, Writing – Review & Editing, Data interpretation, Supervision. Jianshe Chen: Writing – Review & Editing. Rammile Ettelaie: Writing – Review & Editing, Data interpretation.

Funding

Open access funding provided by the University of Natural Resources and Life Sciences Vienna (BOKU).

Declaration of competing interest

The authors declare no conflict of interest.

Appendix A. Supplementary data

Supplementary data to this article can be found online at <https://doi.org/10.1016/j.foodhyd.2021.107054>.

References

Bohrer, B. M. (2019). An investigation of the formulation and nutritional composition of modern meat analogue products. *Food Science and Human Wellness*, 8(4), 320–329.
 Chen, F. L., Wei, Y. M., & Zhang, B. (2011). Chemical cross-linking and molecular aggregation of soybean protein during extrusion cooking at low and high moisture content. *LWT-Food Science and Technology*, 44(4), 957–962.
 Chen, J. (2009). Food oral processing—a review. *Food Hydrocolloids*, 23(1), 1–25.

Chen, J., Chen, X., Zhu, Q., Chen, F., Zhao, X., & Ao, Q. (2013). Determination of the domain structure of the 7S and 11S globulins from soy proteins by XRD and FTIR. *Journal of the Science of Food and Agriculture*, 93(7), 1687–1691.
 Chen, J., & Stokes, J. R. (2012). Rheology and tribology: Two distinctive regimes of food texture sensation. *Trends in Food Science & Technology*, 25(1), 4–12.
 Chen, P., Zhang, L., & Cao, F. (2005). Effects of moisture on glass transition and microstructure of glycerol-plasticized soy protein. *Macromolecular Bioscience*, 5(9), 872–880.
 Chiang, J. H., Loveday, S. M., Hardacre, A. K., & Parker, M. E. (2019). Effects of soy protein to wheat gluten ratio on the physicochemical properties of extruded meat analogues. *Food Structure*, 19, 100102.
 Czichos, H. (2009). *Tribology: A systems approach to the science and technology of friction, lubrication, and wear* (Vol. 1). Elsevier.
 Dankar, I., Pujolà, M., El Omar, F., Sepulcre, F., & Haddarah, A. (2018). Impact of mechanical and microstructural properties of potato puree-food additive complexes on extrusion-based 3D printing. *Food and Bioprocess Technology*, 11(11), 2021–2031.
 Godoi, F. C., Prakash, S., & Bhandari, B. R. (2016). 3D printing technologies applied for food design: Status and prospects. *Journal of Food Engineering*, 179, 44–54.
 Guerrero, P., Retegi, A., Gabilondo, N., & De la Caba, K. (2010). Mechanical and thermal properties of soy protein films processed by casting and compression. *Journal of Food Engineering*, 100(1), 145–151.
 Guinier, A. (1994). *X-ray diffraction in crystals, imperfect crystals, and amorphous bodies*. Courier Corporation.
 Hiiemae, K. M., & Palmer, J. B. (2003). Tongue movements in feeding and speech. *Critical Reviews in Oral Biology & Medicine*, 14(6), 413–429.
 Ilhamto, N. (2012). *Producing in-house pureed food in long-term care* (Doctoral dissertation).
 ISO (International Organization for Standardization). (2012). *ISO 8586. Sensory analysis: General guidelines for the selection, training and monitoring of selected assessors and expert sensory assessors*.
 Kiumarsi, M., Majchrzak, D., Jäger, H., Song, J., Lielig, O., & Shahbazi, M. (2021). Comparative study of instrumental properties and sensory profiling of reduced-fat chocolate containing hydrophobically modified inulin. Part II: Proton mobility, topological, tribological and dynamic sensory properties. *Food Hydrocolloids*, 110, 106144.
 Kiumarsi, M., Majchrzak, D., Yeganehzad, S., Jäger, H., & Shahbazi, M. (2020). Comparative study of instrumental properties and sensory profiling of reduced-fat chocolate containing hydrophobically modified inulin. Part I: Rheological, thermal, structural and external preference mapping. *Food Hydrocolloids*, 104, 105698.
 Kiumarsi, M., Shahbazi, M., Yeganehzad, S., Majchrzak, D., Lielig, O., & Winkeljann, B. (2019). Relation between structural, mechanical and sensory properties of gluten-free bread as affected by modified dietary fibers. *Food Chemistry*, 277, 664–673.
 Kokubun, S., Ratcliffe, L., & Williams, P. A. (2015). The emulsification properties of octenyl- and dodecylsuccinylated inulins. *Food Hydrocolloids*, 50, 145–149.
 Lin, S., Huff, H. E., & Hsieh, F. (2000). Texture and chemical characteristics of soy protein meat analog extruded at high moisture. *Journal of Food Science*, 65(2), 264–269.
 Lipton, J., Arnold, D., Nigl, F., Lopez, N., Cohen, D. L., Norén, N., et al. (2010, August). Multi-material food printing with complex internal structure suitable for conventional post-processing. In *Solid freeform fabrication symposium*, 809–815.
 Liu, K. S., & Hsieh, F. H. (2007). Protein–protein interactions in high moisture-extruded meat analogs and heat-induced soy protein gels. *Journal of the American Oil Chemists' Society*, 84(8), 741–748.
 Liu, Z., Zhang, M., Bhandari, B., & Yang, C. (2018). Impact of rheological properties of mashed potatoes on 3D printing. *Journal of Food Engineering*, 220, 76–82.
 Li, C., Wang, J., Shi, J., Huang, X., Peng, Q., & Xue, F. (2015). Encapsulation of tomato oleoresin using soy protein isolate-gum aracia conjugates as emulsifier and coating materials. *Food Hydrocolloids*, 45, 301–308.
 Majzoobi, M., Shahbazi, M., Farahnaky, A., Rezvani, E., & Schleinig, G. (2013). Effects of high pressure homogenization on the physicochemical properties of corn starch. In *InsideFood Symposium* (pp. 33–35).
 Mantihal, S., Prakash, S., Godoi, F. C., & Bhandari, B. (2017). Optimization of chocolate 3D printing by correlating thermal and flow properties with 3D structure modeling. *Innovative Food Science & Emerging Technologies*, 44, 21–29.
 Miller, J. L., & Watkin, K. L. (1996). The influence of bolus volume and viscosity on anterior lingual force during the oral stage of swallowing. *Dysphagia*, 11(2), 117–124.
 Navazesh, M. (1993). Methods for collecting saliva. *Annals of the New York Academy of Sciences*, 694(1), 72–77.
 Nguyen, P. T., Nguyen, T. A., Bhandari, B., & Prakash, S. (2016). Comparison of solid substrates to differentiate the lubrication property of dairy fluids by tribological measurement. *Journal of Food Engineering*, 185, 1–8.
 Osen, R., Toelstede, S., Wild, F., Eisner, P., & Schweiggert-Weisz, U. (2014). High moisture extrusion cooking of pea protein isolates: Raw material characteristics, extruder responses, and texture properties. *Journal of Food Engineering*, 127, 67–74.
 Owusu-Apenten, R. (2002). *Food protein analysis: Quantitative effects on processing* (Vol. 118). CRC press.
 Pineau, N., Schlich, P., Cordelle, S., Mathonnière, C., Issanchou, S., Imbert, A., & Köster, E. (2009). Temporal Dominance of Sensations: Construction of the TDS curves and comparison with time–intensity. *Food Quality and Preference*, 20(6), 450–455.
 Pulatsu, E., Su, J. W., Lin, J., & Lin, M. (2020). Factors affecting 3D printing and post-processing capacity of cookie dough. *Innovative Food Science & Emerging Technologies*, 61, 102316.

- Shahbazi, M., Ahmadi, S. J., Seif, A., & Rajabzadeh, G. (2016). Carboxymethyl cellulose film modification through surface photo-crosslinking and chemical crosslinking for food packaging applications. *Food Hydrocolloids*, *61*, 378–389.
- Shahbazi, M., & Jäger, H. (2020). Current status in the utilization of biobased polymers for 3D printing process: A systematic review of the materials, processes, and challenges. *ACS Applied Bio Materials*, *4*(1), 325–369.
- Shahbazi, M., Jäger, H., Ahmadi, S. J., & Lacroix, M. (2020). Electron beam crosslinking of alginate/nanoclay ink to improve functional properties of 3D printed hydrogel for removing heavy metal ions. *Carbohydrate Polymers*, 116211.
- Shahbazi, M., Jäger, H., Ettelaie, R., & Chen, J. (2021c). Construction of 3D printed reduced-fat meat analogue by emulsion gels Part I: Flow behaviour, thixotropic feature, and network structure of printable inks. *Food Hydrocolloids*, *120*, 106967.
- Shahbazi, M., Jäger, H., & Ettelaie, R. (2021a). Application of Pickering emulsion and 3D printing for personalized nutrition. Part I: Development of reduced-fat printable cheese analogue ink. *Colloids and Surfaces A: Physicochemical and Engineering Aspects*, 126641.
- Shahbazi, M., Jäger, H., & Ettelaie, R. (2021b). Application of Pickering emulsions in 3D printing of personalized nutrition. Part II: Functional properties of reduced-fat 3D printed cheese analogues. *Colloids and Surfaces A: Physicochemical and Engineering Aspects*, *624*, 126760.
- Shahbazi, M., Majzoobi, M., & Farahnaky, A. (2018a). Impact of shear force on functional properties of native starch and resulting gel and film. *Journal of Food Engineering*, *223*, 10–21.
- Shahbazi, M., Majzoobi, M., & Farahnaky, A. (2018b). Physical modification of starch by high-pressure homogenization for improving functional properties of κ -carrageenan/starch blend film. *Food Hydrocolloids*, *85*, 204–214.
- Sharma, M., Kristo, E., Corredig, M., & Duizer, L. (2017). Effect of hydrocolloid type on texture of pureed carrots: Rheological and sensory measures. *Food Hydrocolloids*, *63*, 478–487.
- Sun, J., Peng, Z., Yan, L., Fuh, J. Y. H., & Hong, G. S. (2015). 3D food printing an innovative way of mass customization in food fabrication. *International Journal of Bioprinting*, *1*(1).
- Szczesniak, A. S. (2002). Texture is a sensory property. *Food Quality and Preference*, *13* (4), 215–225.
- Thiébaud, M., Dumay, E., & Cheftel, J. C. (1996). Influence of process variables on the characteristics of a high moisture fish soy protein mix texturized by extrusion cooking. *LWT-Food Science and Technology*, *29*(5–6), 526–535.
- Van der Linden, D. (2015). *3D Food printing Creating shapes and textures*.
- Zhao, X., Zhu, H., Zhang, B., Chen, J., Ao, Q., & Wang, X. (2015). XRD, SEM, and XPS analysis of soybean protein powders obtained through extraction involving reverse micelles. *Journal of the American Oil Chemists' Society*, *92*(7), 975–983.